POLITECNICO DI TORINO
Repository ISTITUZIONALE

Modelling cell migration strategies in the extracellular matrix

Original
Modelling cell migration strategies in the extracellular matrix / Painter, K. J.. - In: JOURNAL OF MATHEMATICAL BIOLOGY. - ISSN 0303-6812. - 58:4-5(2009), pp. 511-543. [10.1007/s00285-008-0217-8]

Availability:
This version is available at: 11583/2973884 since: 2022-12-15T14:28:48Z

Publisher:
Springer

Published
DOI:10.1007/s00285-008-0217-8

Terms of use:

This article is made available under terms and conditions as specified in the corresponding bibliographic description in the repository

Publisher copyright

(Article begins on next page)

23 April 2024

Journal of Mathematical Biology manuscript No.
(will be inserted by the editor)

K. J. Painter

Modelling cell migration strategies in the extracellular matrix

the date of receipt and acceptance should be inserted later

Abstract: The extracellular matrix (ECM) is a highly organised structure with the capacity to direct cell migration through their tendency to follow matrix fibres, a process known as *contact guidance*. Amoeboid cell populations migrate in the ECM by making frequent shape changes and have minimal impact on its structure. Mesenchymal cells actively remodel the matrix to generate the space in which they can move. In this paper, these different types of movement are studied through simulation of a continuous transport model. It is shown that the process of contact guidance in a structured ECM can spatially organise cell populations. Furthermore, when combined with ECM remodelling, it can give rise to cellular pattern formation in the form of "cell-chains" or networks without additional environmental cues such as chemoattractants. These results are applied to a simple model for tumour invasion where it is shown that the interactions between invading cells and the ECM structure surrounding the tumour can have a profound impact on the pattern and rate of cell infiltration, including the formation of characteristic "fingering" patterns. The results are further discussed in the context of a variety of relevant processes during embryonic and adult stages.

1 Introduction

Cell migration plays a fundamental role in tissue development, maintenance and breakdown. During embryonic growth, a variety of processes including gastrulation, neural crest migration, axonal guidance and tissue formation require precisely coordinated cell movements, either as individuals or as a collective cell group (for a review, see Locascio and Nieto 2001). In the adult organism, cell migration is a crucial component of tissue homeostasis, tissue repair and the immune response. Mutations arising in cancerous cells may lead to their uncontrolled migration and subsequent invasion into the surrounding healthy tissue (e.g. Mareel and Leroy 2003). A range of external cues impart information to the cells that regulates their movement, including long range diffusible chemicals (e.g. chemoattractants), contact with membrane bound molecules on neighbouring cells (e.g. cell-cell adhesion and contact inhibition) and contact with the extracellular matrix (ECM) surrounding the cells. In this paper we shall explore the role of interactions between cells and the matrix in directing cell movement.

The ECM comprises a highly organised meshwork that forms a substantial part of tissues: in the case of connective tissue such as the dermal skin layer, up to 70%. A variety of proteins and polysacharrides make up the matrix, including collagen, fibronectin and hyaluronan. The characteristic rope-like meshwork of the ECM is principally formed from collagen proteins which can self-assemble to form collagen fibrils 10-300nm in diameter and 100s of micrometers in length (Alberts *et al.* 1994; Hay 1991). In addition to

Department of Mathematics and Maxwell Institute for Mathematical Sciences, Heriot-Watt University, Edinburgh, EH14 4AS, UK, E-mail: painter@ma.hw.ac.uk

acting as a supporting structure to the cells, via its expression of a wide variety of chemical cues the ECM plays a major regulatory role in all facets of cell behaviour, including differentiation, proliferation and migration. The latter is strictly controlled by the ECM, which has the ability to either facilitate or prevent cell movement: fibroblasts and leukocytes utilise the ECM for movement as part of normal physiological responses in tissue repair and inflammation. In addition to providing a "scaffold" to which cells can anchor and generate force, the ECM provides guidance information to the cells either indirectly through matrix bound adhesive molecules (haptotaxis) or directly through cells following along matrix fibres, a process known as contact guidance (Dunn and Heath 1976). To other cell types, such as epithelial cells, the ECM presents a physical and chemical barrier to movement, thereby playing an important role in maintaining tissue integrity.

1.1 Migration strategies in the ECM

A variety of motility types have been identified by cells in the ECM (Friedl 2004). Broadly, these can be classified as either individual or collective. In the former, cells migrate as single elements and form only transient contacts with other migrating cells. In the latter, migration occurs as a cluster or sheet of cells maintained by strong adhesive contacts. In this paper the focus will be on individual cell migration.

Individual cell migration can be further subdivided into two classes: amoeboid and mesenchymal, (Friedl 2004). Mesenchymal, utilised by fibroblasts, certain tumour cells and neutrophils, is slow (0.1-2 μm/min) and cells move through continuous formation and breakage of "focal adhesions" between their membrane and the matrix. To create the necessary space to move, cells cut a hole in the ECM through the production and secretion of matrix degrading proteins (or proteolytic enzymes) such as members of the MMP family. Matrix degradation occurs in either a contact or non-contact dependent manner: in the former (pericellular proteolysis) the proteolytic enzymes are recruited to focal adhesions at the leading edge of a migrating cell where they act on those fibres directly in its path. In non-contact dependent proteolysis, enzymes are secreted by the cell into the extracellular environment where they diffuse and degrade distant matrix. As a result of remodelling, a matrix defect arises (or cell-path), (Friedl *et al.* 1997; Murphy and Gavrilovic 1999; Wolf *et al.* 2003b) comprised of fibres predominantly oriented along the path of cell migration, Figure 1 (b). The functional role (if any) of such cell-paths is unclear: imaging studies reveal that cells frequently migrate onto and along previously formed paths, occasionally forming "cell-chains", Figure 1 (c). Migrating cell-chains have been observed in a variety of biological processes: the formation of chains during the early stages of neural crest cell migration (Kulesa and Fraser 1998; Jacques *et al.* 1998) suggests a potential role in embryonic patterning whilst their appearance in cancer populations (Friedl *et al.* 1997) indicates a capacity to facilitate tumour spread through the creation of invasive pathways.

Amoeboid migration, named because of its mechanistic similarity to the movement of cellular slime molds, occurs in T-lymphocytes (Wolf *et al.* 2003a), certain carcinoma cells (Wang *et al.* 2002) and stem cells (Francis *et al.* 2002). Cells form only transient contacts with the ECM and migrate by making frequent changes in direction and shape deformation (see Figure 1 (a)) to squeeze through small holes in the matrix (Wolf *et al.* 2003a), thereby dispensing of the need for proteolytic action and permitting faster migration speeds, between 2 and 30 μm/min.

As observed above, the ECM is known to impart directional information to cells through their tendency to follow individual fibrils, a process known as contact guidance (Dunn and Heath 1976; Guido and Tranquillo 1993). Contact guidance has been observed in both amoeboid (e.g. Wolf *et al.* 2003a) and mesenchymal cell populations (Guido and Tranquillo 1993) and has been proposed to play an important role in cell migration in development and the adult. A number of studies have implicated contact guidance during the patterning of the pectoral fin bud of the teleost embryo: upon migrating into the fin, cells become contact-aligned with the highly organised fibril structure which guides them to their final location (Wood and Thorogood 1984; Thorogood and Wood 1987). Contact guidance has also been suggested as playing a role in the *in vivo* guidance of neural crest cells (Newgreen 1989) whilst in the adult it has been demonstrated by both immune cells (Wilkinson and Lackie 1983) and fibroblast cells responsible for tissue repair following injury (Guido and Tranquillo 1993).

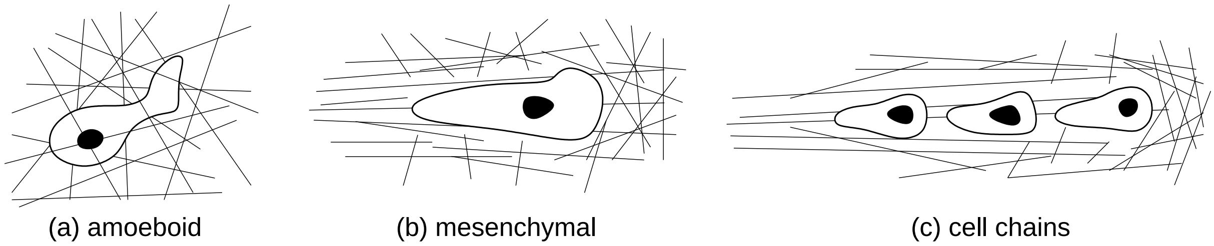

Fig. 1 Schematic of different types of individual cell migration. (a) In amoeboid migration, cells squeeze through the matrix but have negligible impact on its overall structure. (b) Mesenchymal migration involves significant matrix remodelling, leaving a trail of aligned matrix along the cell path. (c) Cell chains in mesenchymal populations. Adapted from Friedl (2004).

1.2 Previous Modelling

The effects of interactions between cell movement and the organisation/alignment of an underlying matrix have been investigated by a number of previous authors applied to various biological systems. The model developed in this paper builds on earlier work in Hillen (2006). There, a transport model was formulated to describe mesenchymal migration of cells in tissues, incorporating the twin actions of contact guidance/fibre following by the cells and matrix remodelling. Hillen focusses on the corresponding macroscopic (i.e. diffusion) limit for the various transport models above, the impact of contact guidance leading to an anisotropic diffusion tensor that depends on the underlying structure of the ECM. An extension of the modelling in Hillen (2006) to incorporate cell-cell interactions and chemotaxis has been presented in Chauviere *et al.* (2007). In the modelling presented later, numerical simulations of an underlying transport model similar to that proposed in Hillen (2006) are conducted and their significance for different types of biological movement discussed. A transport-based model for contact guidance has also been developed and studied by Dickinson (Dickinson 1997, 2000). Barocas and Tranquillo developed the "anisotropic biphasic theory" by considering mass and momentum balance equations between tissue-cell phase and interstitial fluid phase that incorporate cell and fibre alignment (Barocas and Tranquillo 1997).

A number of models incorporating contact guidance have been developed by Sherratt, Dallon and others in the context of understanding fibroblast–ECM interactions during scarring/wound healing. These works can be split into two groups. In the first, hybrid discrete-continuous models were investigated in which fibroblasts were modelled as discrete objects whilst the matrix and other factors (e.g. chemoattractants) were modelled as continuous variables (Dallon *et al.* 1999, 2001; McDougall *et al.* 2006). Contact guidance was introduced by assuming the fibroblast cells orient according to the underlying collagen matrix (modelled as a single dominant angle). In the second set of papers, continuum description were considered for both the cells and the matrix using either reaction-diffusion equations (Olsen *et al.* 1998, 1999) or integro-pde systems (Dallon and Sherratt 1998, 2000). The latter have also been developed to model the alignment of objects (such as fibroblast cells), however here the alignment was initiated through direct cell-cell contact rather than contact guidance with a matrix (Mogilner and Edelstein-Keshet 1996; Mogilner *et al.* 1996).

1.3 Outline

In this paper a model is described for different types of cell migration in the ECM. The aim of the paper is to address the following questions.

- How does the architecture of the ECM alter the macroscopic organisation of cells migrating through contact guidance?
- How does feedback between contact-guided migration and matrix reorganisation by the cells alter patterning? In particular, can the mesenchymal "cell-chains" be generated through these actions alone, or are additional mechanisms necessary (e.g. cell-cell adhesion)?
- How do the interactions between cells and the aligned structure of the ECM alter patterns of infiltration during tumour invasion?

In Section 2 we develop a model based on the transport equation approach recently developed in Hillen (2006). In Section 3, we apply this model to amoeboid migration and demonstrate that a structured ECM can induce cell aggregation and organisation. In Section 4 we model mesenchymal migration by adding matrix remodelling by the cells. The combined action of contact guidance and matrix remodelling is shown to lead to cell-chains and network pattern formation. In Section 5 a simple model is developed to described tumour invasion into a structured ECM. The type of cell migration and the alignment of the ECM are demonstrated to have a potentially large impact on the rate and manner of tumour invasion, leading to "fingering" type behaviour. Finally, we discuss the findings in the context of physiological examples of cell migration.

2 Modelling

It is assumed that cells migrate as a "run and tumble" process in which periods of running with fixed orientation are punctuated at discrete times by an instantaneous sensing of the environment and reorientation. The paradigm for this type of motion is the flagellar bacteria *E. coli* (Alberts *et al.* 1994), yet it can reasonably approximate other types of motion, such as eukaryotic cell movement, through the specific functional forms describing the speed and turning of cells. In principle, any number of external factors can be incorporated into the sensing, for example tactic cues. The focus here will be on the influence of the ECM.

The model is formulated and solved in the form of a transport equation in which continuous cell distributions of varying velocities are tracked in space. Reorientations between velocities are selected according to a turning function/probability distribution depending on the environmental variables. In cell movement, this approach has been extensively utilised to model chemotaxis (e.g. see Othmer *et al.* 1988; Hillen 2002). The continuous transport equation approach adopts a middle ground between microscopic/discrete cell approaches and a truly macroscopic representation: while the model is formulated using a microscopic description for cell motion, the outputs are macroscopic properties such as cellular densities and matrix distributions. This has led to their description as "mesoscopic" in the literature (Hillen 2006). Furthermore, the continuous nature of the equations offers a greater degree of analytical tractability than a discrete approach.

2.1 General Model

We consider the motion of an individual cell in some space Ω to follow a velocity-jump process (Othmer *et al.* 1988), that is, cells move by smooth running interrupted at discrete times by an instantaneous reorientation. In general, the choice of a new velocity and the average runtime between reorientations will depend on environmental factors. The velocity-jump process is formulated as follows

$$c(\mathbf{x},\mathbf{v},t)_t + \nabla\cdot\mathbf{v}c(\mathbf{x},\mathbf{v},t) = -\mu c(\mathbf{x},\mathbf{v},t) + \mu\int_V T(\mathbf{v},\mathbf{v}')c(\mathbf{x},\mathbf{v}',t)d\mathbf{v}'$$
$$\mathbf{m}(\mathbf{x},\phi,t)_t = -\nabla\mathbf{J_m} + f(c,\mathbf{m})$$

In the first equation above, $c(\mathbf{x},\mathbf{v},t)$ can be interpreted either as the probability distribution for a cell to be at position $\mathbf{x}$ and velocity $\mathbf{v}$ at time t or, if it is assumed that there are no direct cell-cell interactions, as the density of cells at position $\mathbf{x}$ with velocity $\mathbf{v}$. The first term on the right hand side describes turning of cells away from velocity $\mathbf{v}$ with a *turning rate* μ (1/mean run-time) that may depend on the environmental factors. The integral term calculates the rate at which cells reorient into velocity $\mathbf{v}$ given previous velocity $\mathbf{v}'$, summed over an appropriate velocity space V. The function $T(\mathbf{v},\mathbf{v}')$ defines a probability distribution for a cell with previous velocity $\mathbf{v}'$ to choose new velocity $\mathbf{v}$. Clearly cell conservation dictates that

$$\int_V T(\mathbf{v},\mathbf{v}')d\mathbf{v}' = 1\,.$$

Notice that the above excludes cellular kinetics to focus on movement.

The second equation above encodes the dynamics for the environmental variables: in the application considered here this should include, at the very least, a representation for the extracellular matrix. Additional factors, such as secreted chemical factors, may be included as appropriate. $\mathbf{J_m}$ describes flux terms while $f(c, \mathbf{m})$ describes the kinetics.

2.2 Simplified model

The above model has been posed in general form to illustrate the transport equation approach. It can be applied to describe different types of cell movement through the specific choices for turning rates, turning functions and environmental variables. Direct numerical exploration is challenging: simulation in 2D will alone require discretisation of a 4-dimensional space since cell densities are tracked in both space and velocity.

To develop a model in a manner more amenable to numerical analysis, a number of simplifying assumptions are made. Firstly, we restrict cell migration to a two-dimensional rectangular domain. Although cell migration *in vivo* is, obviously, a three-dimensional process, it is believed that the restriction to 2D will admit crucial insight. Secondly, it is assumed that the velocity of a cell between reorientations at times t_j and t_{j+1} is given by

$$\mathbf{v} = s(\mathbf{m})(\cos\theta(t_j), \sin\theta(t_j))$$

where $s(\mathbf{m})$ is the instantaneous cell speed and $\theta(t_j) \in (-\pi, \pi]$ is its orientation, chosen at the time of the previous reorientation. The above implicitly assumes that cell direction remains fixed between sensing whilst the speed varies continuously according to the environment. For the majority of this paper an even simpler case will be considered in which $s(\mathbf{m}) = s_0$. These approximations reduce the dimensionality by allowing cell distribution to be tracked in space and angle only. A further restriction is that the runtime between reorientations is presumed independent of environmental variables, although more realistically this should also depend on the matrix: for example, if cells encounter a large obstacle, they may be forced to reorient.

As described earlier, the ECM *in vivo* comprises a multitude of proteins and polysachharides organised into a highly structured meshwork. In collagenous matrix, such as the dermis, these may form long fibres up to several 100 μms in length. We represent the matrix in the model by condensing it into a single generic variable $m(\mathbf{x}, \phi, t)$ representing a fibrous ECM in which the matrix at each point in space is recorded as a distribution of fibres of varying orientation. Fibres are assumed not to have a specific polarity (i.e. there is no "up" or "down" a matrix fibre) and thus the angular distribution for matrix varies between $-\pi$ and 0. At present, no further environmental variables are considered. *In vivo*, the situation is more complex. For example, interactions between cells and the matrix are mediated by a variety of secreted and membrane bound molecules, such as proteolytic enzymes, while guidance cues including chemotactic and haptotactic factors also play a role in cell orientation.

For simplicity, it is assumed that the cell action on the matrix is local, that is we take $\mathbf{J_m} = 0$. This can be partially justified if the major contribution to remodelling is via pericellular proteolysis whereby enzyme action is mediated at the cell membrane (Murphy and Gavrilovic 1999). However, it is clearly a simplification of the true situation where cells can both secrete diffusible enzymes which act over a longer range and alter the matrix nonlocally through mechanical forces. As above, the simplification here is intended to limit the model to a manageable form and understand how interactions between cell guidance by the matrix and matrix remodelling by the cells shape cell movement pathways. Clearly, a focus for future modelling work should be a more realistic representation of the nonlocal interactions between cells and the matrix.

Under the various assumptions above, the equations are reduced to

$$c(\mathbf{x}, \theta, t)_t + \nabla \cdot \mathbf{v} c(\mathbf{x}, \theta, t) = -\mu c(\mathbf{x}, \theta, t) + \mu \int_{-\pi}^{\pi} T(\theta, \theta') c(\mathbf{x}, \theta', t) d\theta' \,, \tag{1}$$

$$m(\mathbf{x}, \phi, t)_t = f(c, m) \,. \tag{2}$$

where $c(\mathbf{x}, \theta, t)$ describes the density of cells with orientation $\theta \in (-\pi, \pi]$ and $m(\mathbf{x}, \phi, t)$ describes the distribution of matrix fibres for $\phi \in (-\pi, 0]$. It is assumed that cells are restricted to a 2D rectangular domain $\Omega = [0, L_x] \times [0, L_y]$ with periodic boundary conditions, except where stated. Note that cell conservation now requires

$$\int_{-\pi}^{\pi} T(\theta, \theta')d\theta' = 1 \,.$$

2.3 Numerical methods

A detailed investigation into the numerical scheme will be presented separately and we confine ourselves here to a brief summary of the method invoked. In the numerical simulations that follow, a Method of Lines approach is used to solve the generic equations (1-2) in which spatial and angular terms are initially discretised to yield a large system of time-dependent ODEs (the MOL-ODEs). Spatial terms comprise of an advective term representing cell movement and are approximated in conservative form using a finite volume method. To ensure reasonable spatial accuracy, the discretisation of the advective term utilises a third-order upwinding scheme augmented with a flux-limiting scheme to ensure positivity of solutions. Angular terms comprise of an integral term (representing cell-turning) which is approximated by discretisation in angle and employing a trapezoidal scheme. Integration in time of the MOL-ODE systems has been performed using both explicit and implicit schemes. The explicit scheme (forward euler) is capable of handling the large system of equations generated by the spatial/angular discretisation yet necessitates a small time step for stable and accurate solution. To provide an efficient and robust scheme capable of solving what may, in general, be stiff systems of equations we have also used the ROWMAP stiff systems integrator (Weiner *et al.* 1997). Similar approaches to those described above have been developed in other models of cell movement (e.g. see Gerisch and Chaplain 2007). Tests using the two time iteration methods yield equivalent results and simulations have been performed across a range of discretisation steps.

2.4 Representation of the data

Despite the number of simplifying assumptions, Equations (1)–(2) are capable of producing a vast amount of data, including cell/matrix density distributions in 2D space, angle and time. To portray this information, we define the following “observables”, listed in Table 1.

- *macroscopic cell/matrix densities* , the total density at $\mathbf{x}$ summed across all cell/matrix orientations. For the cells,

$$\overline{c}(\mathbf{x}, t) = \int_{-\pi}^{\pi} c(\mathbf{x}, \theta, t)d\theta$$

  with a similar definition for the matrix.
- *cell/matrix alignment*, a measure of the direction and strength of cell/matrix alignment at $\mathbf{x}$. For the cells, this is computed as the vector

$$\overrightarrow{c}(\mathbf{x}, t) = \int_{-\pi}^{\pi} \left(c(\mathbf{x}, \theta, t)\cos\theta, c(\mathbf{x}, \theta, t)\sin\theta\right) d\theta \,. \tag{3}$$

The above is represented graphically by plotting its argument, $\Theta(\mathbf{x}, t)(\in (-\pi, \pi])$, and magnitude, $c_L(\mathbf{x}, t) = \|\overrightarrow{c}\|$. This process, while providing information on the net movement of the population, inevitably oversimplifies the characteristic cell movement patterns. For example, for symmetric cell distributions (e.g. cells migrating uniformly in all directions or equal cell densities migrating in opposite directions) we must have $\overrightarrow{c} = 0$. In any such cases, an alternative measure will be employed to indicate the dominant orientations of the cells.

For the matrix alignment a similar quantity $\overrightarrow{m}(\mathbf{x}, t)$ is obtained, modified to take the bidirectional nature of the fibres into account (i.e. their distribution lies only between $-\pi$ and 0). Firstly, we rescale by introducing the variable $\alpha = 2\phi + \pi$ and calculate

$$\int_{-\pi}^{\pi} \left(m(\mathbf{x}, \alpha, t)\cos\alpha, m(\mathbf{x}, \alpha, t)\sin\alpha\right) d\alpha \,.$$

Notation/Definition	Interpretation
$\overline{c} = \int_{-\pi}^{\pi} c(\mathbf{x}, \theta, t) d\theta$	Macroscopic cell density
$\overline{m} = \int_{-\pi}^{0} m(\mathbf{x}, \phi, t) d\phi$	Macroscopic matrix density
$\Theta = \arg \overrightarrow{c}(\mathbf{x}, t)$	Dominant local cell orientation
$\Phi = \arg \overrightarrow{m}(\mathbf{x}, t)$	Dominant local matrix orientation
$c_L = \lVert\overrightarrow{c}(\mathbf{x}, t)\rVert$	Strength of local cell alignment
$m_L = \lVert\overrightarrow{m}(\mathbf{x}, t)\rVert$	Strength of local matrix alignment

Table 1 List of functions and their interpretations employed in data representation.

The above quantity yields a vector with argument $A(\mathbf{x}, t)$ lying in $(-\pi, \pi]$ due to the rescaling of ϕ. To obtain the vector with the appropriate argument between $-\pi$ and 0 we perform the reverse scaling using $A = 2\Phi + \pi$ to obtain the matrix alignment vector $\overrightarrow{m}(\mathbf{x}, t) = m_L(\cos\Phi, \sin\Phi)$.

To demonstrate the general suitability of this measure, we consider the two matrix distributions in Figure 2 (b) and (c). The matrix in (b) is randomly distributed in $(-\pi, 0]$, normalised such that $\overline{m} = 1$. The dominant matrix orientation is determined to be $\Phi = -3.04$ radians, although for different sets of random initial data this varies uniformly in $(-\pi, 0]$. The strength of matrix alignment m_L is small ($O(10^{-3})$), indicative that all matrix orientations are almost equally represented. For the matrix distribution in (c), the macroscopic matrix density is the same as above, $\overline{m} = 1$, however now the orientation of the fibres is such that $\Phi = -\pi/4$ while m_L is large (≈ 0.8), representing a highly aligned matrix.

3 Rules for "amoeboid" migration

3.1 Model formulation

Amoeboid migration is carried out by hematopoietic stem cells (Francis *et al.* 2002), T-cells (Wolf *et al.* 2003a) and certain cancer cells (Wang *et al.* 2002). Migrating amoeboid cells can squeeze through small holes in the matrix, thereby dispensing of the need to degrade it by proteolysis (Wolf *et al.* 2003a): experimental studies indicates the matrix is only *transiently* distorted as cells squeeze through it and the ECM rapidly returns to its previous state. The brief contact between the ECM and cells permits rapid cell movement (2-30 μm/min) and cells demonstrate frequent turns, in part due to their need to circumnavigate large obstacles in the matrix (i.e. where they are unable to squeeze through).

From the perspective here, amoeboid-style migration offers the opportunity to study how the ECM can dictate global cell migration pathways: the "amoeboid-type" cells we describe in the model are assumed to actively respond to the matrix through their tendency to follow fibres (i.e. contact guidance), but do not fundamentally alter its structure. The model is based on the following set of assumptions:

(A1) negligible matrix remodelling,
(A2) frequent turning and high cell speeds,
(A3) contact guided migration along fibres.

(A1) implies that matrix dynamics can be ignored and therefore the ECM is prescribed through its initial distribution. (A2) dictates the parameters for the cell speed and turning rate in the transport models: default values for these parameters are listed in Table 2. In the initial study it is assumed for simplicity that cells move with a constant speed s_0 and hence the velocity for cells migrating in direction θ is given by $\mathbf{v} = s_0(\cos\theta, \sin\theta)$ – more realistically the speed will be a function of the matrix (e.g. see Perumpanani and Byrne 1999; Gaudet *et al.* 2003).

(A3) dictates the choice of probability distribution for selecting a new cell direction and, to model contact guidance, it is assumed that cells bias their direction according to the local distribution of m (see

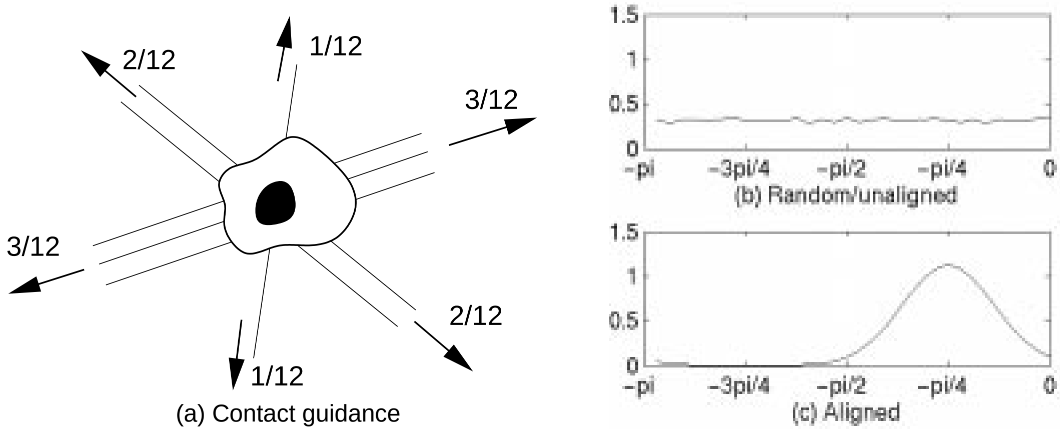

Fig. 2 (a) Schematic illustrating the modelling of contact guidance. The fractions give the probabilities of migrating in each of the indicated directions for the underlying matrix, based on Equation (4) with $b = 1$. (b)–(c) The two types of local angular distribution of matrix fibres employed in the amoeboid model simulations. In (c) the dominant local matrix orientation is $-\pi/4$.

Figure 2 (a)):

$$T(\theta, \theta') = \begin{cases} \dfrac{1-b}{2\pi} + b\dfrac{m(\theta)}{2\overline{m}} & \text{if} \quad \theta \in (-\pi, 0] \\ \dfrac{1-b}{2\pi} + b\dfrac{m(\theta-\pi)}{2\overline{m}} & \text{if} \quad \theta \in (0, \pi] \end{cases} \tag{4}$$

The above takes into account that fibres are bi-directional and cells are unable to resolve between "up" and "down" a fibre. $b \in [0, 1]$ is a parameter reflecting the degree to which random effects and contact guidance bias the choice of direction. A straightforward calculation shows that the above satisfies the cell conservation condition, i.e. $\int_{-\pi}^{\pi} T\, d\theta = 1$. The above, with the simple addition of the random component, is based on the assumptions in Hillen (2006). This relatively simple model for contact guidance is based on phenomological grounds, rather than a precise mechanistic/biochemical basis, on the pretext of focusing on how interactions between cells and the matrix drive global organisation. A more realistic model would entail incorporation of the effects of mechanical forces and the biochemical pathways leading to cell-matrix coupling.

Further factors that influence cell guidance are neglected at present. For example, it is known that many migrating cells show orientational persistence as a result of a polarisation process that generates a cell *leading edge* (Lauffenburger and Horwitz 1996). While it is possible to extend the modelling to integrate persistence — for example by adapting the functional form in equation (4) to include appropriate dependence on the prior direction θ' — an explicit incorporation would introduce further parameters and increase the complexity of the model. Therefore, at present, any persistence of the cells has been absorbed into the mean run-time parameter. Preliminary simulations indicate that a specific functional representation of persistence does not yield greatly different qualitative behaviour, although a more detailed exploration needs to be conducted. On the same grounds, we exclude the role of chemical signals such as chemotactic or haptotactic cues; the model system can therefore perhaps be most closely compared to an *in vitro* system in which cells migrate in a controlled collagen gel assay.

In summary, for the amoeboid model we solve equations (1)–(2) with turning function (4) and zero matrix dynamics, $f = 0$ in (2). The transport equation is given by

$$c(\mathbf{x}, \theta, t)_t + s_0 \nabla \cdot c(\mathbf{x}, \theta, t)(\cos\theta, \sin\theta) = -\mu c(\mathbf{x}, \theta, t) + \mu \int_{-\pi}^{\pi} T(\theta, \theta') c(\mathbf{x}, \theta', t) d\theta' \tag{5}$$

with a prescribed matrix distribution $m(\mathbf{x}, \phi, 0)$. Except where stated, parameters are selected from the "amoeboid" column in Table 2. Clearly, initial conditions for the matrix may play a huge role on the cellular dynamics and we expand on this in the following section.

Parameter	Interpretation	Amoeboid	Mesenchymal
s_0	mean speed (μm/min)	10.0 see[1]	0.5 see[1]
μ	turning rate (/min)	1.0 see[3]	0.05 see[2]
b	contact guidance strength	1 see[5]	1 see[5]
δ	matrix remodelling rate	n/a see[4]	0.1 see[5]

Table 2 Default values for the main model parameters. Notes: [1] from Friedl *et al.* (1998). [2] from Wang *et al.* (2001). [3] a literature source for this value has not been determined, however studies of cell paths in Friedl *et al.* (1998) indicate a short time; [4] matrix degradation is assumed to be negligible for amoeboid migrating cells (Wolf *et al.* 2003a). [5] parameter values for "phenomological" parameters are undetermined – parameter sensitivity analysis will be applied.

3.2 Cell guidance under varying ECM architecture

3.2.1 Initial matrix distribution

The structure of the ECM varies considerably within a single tissue or from one tissue to another. For cells exhibiting contact guidance, this may have considerable impact on global movement patterns and this is investigated through simulation of the amoeboid model. We consider the following generic forms:

(E1) an unaligned or random ECM, i.e. no dominant fibre orientation, see Figure 3 (a1);
(E2) a globally aligned ECM, i.e. fibres predominantly oriented in a single direction, Figure 3 (b1);
(E3) mixed ECM (combinations of (E1) and (E2)) Figure 3 (c1)–(d1);
(E4) radially oriented ECM, Figure 3 (e1).

All of the above matrix types are relevant to different tissues *in vivo*. Studies of extracellular matrix during embryonic development shows a high degree of organisation: for example, the globally aligned structure of the tail fin in fish (Wood and Thorogood 1984; Thorogood and Wood 1987) and the structure of the ECM surrounding the neural crest (Newgreen 1989). In adults, the matrix surrounding the antigen-processing domains inside Peyer's patches (part of the lymphoid tissue) is highly organised with matrix fibres radiating out from the centre (Ohtsuka *et al.* 1992). Transitions between different types of ECM occur in numerous examples. For example, ultrastructural studies of articular cartilage reveal the matrix is organised into a layered structure: in the outer (tangential) layer, matrix is highly aligned with the fibres running parallel to the articular surface, in the intermediate layer the matrix has a more isotropic structure with little alignment of the fibres whilst in the deeper matrix fibres are again aligned, but this time orthogonally to the articular surface (Hughes *et al.* 2005). Highly varying ECM structure can also be observed in sections of the dermal skin layer (Tsuji 1982). Dermal skin undergoes changes during aging: while the matrix of younger dermal skin is relatively dense, the number of crosslinks decreases with age (Imayama and Braverman 1989) as it takes on an increasingly tortuous nature.

To describe the various matrix types we must specify appropriate angular distributions of the fibres. We assume no spatial variation of the macroscopic matrix density, normalised to $\overline{m}(\mathbf{x}, 0) = 1$, corresponding to a uniform matrix density. The distribution of fibres at $\mathbf{x}$ is assumed to belong to one of the following types:

- a *random local distribution*, in which fibres are uniformly distributed in $(-\pi, 0]$, subject to a small angularly random perturbation (Figure 2 (a));
- an *aligned local distribution* in which fibres are distributed with a Gaussian-type curve centred on a predefined dominant local matrix orientation (Figure 2 (b)).

We plot the data to describe the various matrix types (E1)–(E4) in Figure 3 (a2)–(e2). Represented in the plots are the dominant local matrix orientation (Φ), indicated by the line, and the strength of matrix alignment (m_L), indicated by the grayscale.

Note that the generic phenotypes (E1)–(E4) may equally be represented with other distributions: numerical simulations indicate that only the quantitative behaviour of solutions is affected under such

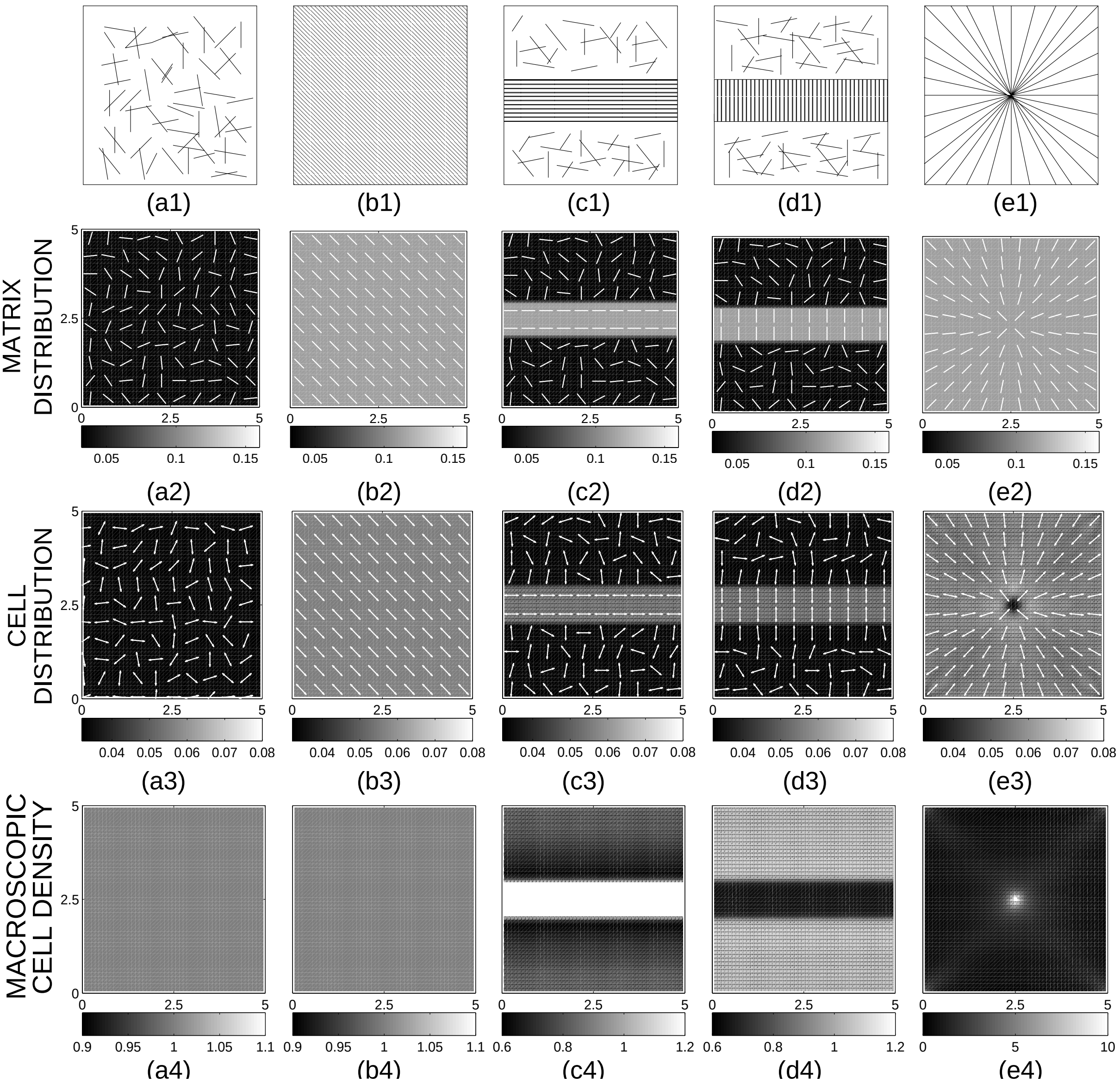

Fig. 3 2D numerical simulations of the transport model for amoeboid migration. (a1)–(e1) schematic showing the matrix structure; (a2)–(e2) Matrix alignment. (a3)–(e3) Cell alignment after 3 hours simulation time. (a4)–(e4) Macroscopic cell density after 3 hours simulation time. Numerical details: space scale $1 = 100\mu$m, numerical simulations use a 50×50 discretisation over space and a 64 (32) point discretisation for the cell (matrix) angle. A larger version of this figure, which shows more clearly the arrowheads in row 3, is available in the supplementary material.

modifications. Situations where the matrix has a specific geometric structure can also be modelled by appropriate alteration of the local fibre distribution, for example if the matrix comprises of an interlocking network of orthogonally oriented fibres.

3.2.2 Numerical simulations

Equation (5) is solved numerically on a grid of size $500 \times 500\,\mu\mathrm{m}^2$, subject to each of the matrix types represented in Figure 3. Except where stated, an initially uniform distribution of cells across both space and orientation is assumed, i.e. $c(\mathbf{x}, \theta, 0) = 1/2\pi$ (and hence $\bar{c}(\mathbf{x}, 0) = 1$). For these and the rest of the

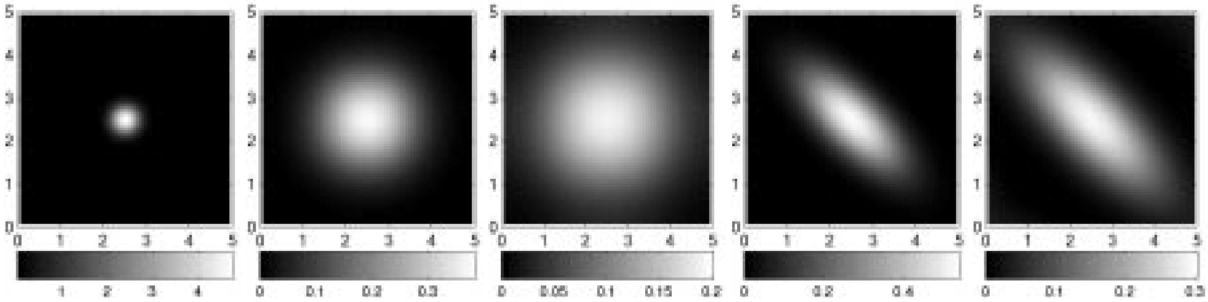

Fig. 4 Simulations illustrating isotropic/anisotropic spread of the cell population under matrix types (E1) and (E2). (a) Initial macroscopic cell density (note that cells are uniformly distributed in orientation). (b) Macroscopic cell density after 60 and 120 minutes for cells migrating in matrix type (E1). (c) Macroscopic cell density after 60 and 120 minutes for cells migrating in matrix type (E2). Parameters/discretisation details as in Figure 3.

simulations in Sections 3 and 4 we shall employ periodic boundary conditions. Parameter values are taken from the default values listed in Table 2 and the equations are solved up until $t = 3$ hours, at which point solutions have evolved close to a steady-state distribution. The cell density distributions are plotted in the bottom two rows of Figure 3. Note that for the cell alignment here we do not employ the measures of cell alignment derived from Equation (3): the bidirectional nature of the fibres results in symmetric cell distributions with approximately equal densities of cells migrating in opposite directions. Thus the vector (3) gives $\overrightarrow{c} \approx 0$ and hence limited information on the local cell alignment. For this figure, we therefore instead calculate the arguments of the local maxima in the cell distribution and plot these using the double arrowheads in Figure 3, row 3.

With the random matrix (E1) there is no discernible change in the cell distribution and they remain (subject to the small random perturbation of the matrix distribution) uniformly distributed in space and orientation (Figures 3 (a3) and (a4)). Cell movement for (E1) is essentially an unbiased random walk, resulting in an isotropic diffusion process at a macroscopic level: numerical simulations for a population of cells initially concentrated in the centre of domain demonstrate uniform radial spread (Figure 4 (b)). For a globally-oriented cell matrix (E2) the impact of contact guidance is demonstrated through the alignment of cells to the underlying matrix (Figure 3 (b3)). With no spatial variation of the matrix organisation, macroscopic cell densities $\overline{c}$ remain uniform (Fig. 3 (b4)). Contact alignment here results in an anisotropic diffusion process at the macroscopic level: radial spread of a population of cells shows enhanced movement along the direction of fibre alignment, Figure 4 (c).

In Figures 3 (c)–(d) data is plotted for two mixed matrix types. In Figure 3 (c), a strip of oriented matrix (type (E2)) is positioned within a non-oriented matrix (type (E1)), with fibres in the strip predominantly aligned parallel to it. Cells demonstrate a high degree of orientation when positioned on the strip, as can be predicted from the above results. Yet a difference now emerges in the macroscopic cell density $\overline{c}$, which demonstrates increased cellular density on the strip (c4). Intuitively, this arises through cells migrating into the aligned region and becoming "trapped". The significance of the ECM arrangement is appreciated by considering the alternative matrix in which fibres in the strip are predominantly aligned orthogonal to it, Figure 3 (d). Cells that migrate onto the strip are quickly transported across it, resulting in a lowering of the macroscopic cell density, $\overline{c}$, on the strip (d4). These two simulations indicate the capacity of an organised ECM to dictate cell patterning: the spatial organisation of the cells is strongly influenced by the underlying ECM. A further test of this capacity is shown using the matrix type (E5) in which fibres are aligned radially. Simulations (Figure 3 (e)) indicate that the cell population can be induced to colocalise at the centre of the grid solely through the action of matrix fibril following, i.e. there is no necessity for an additional orientational cue, such as a diffusible chemoattractant source.

Alterations in the cell speed, s_0, and turning rate, μ, alter the timescale of patterning and the quantitative distribution of cells, but do not impact on their qualitative behaviour. Alterations in the value of b have a greater impact on the patterns: for $b = 0$ there is no contact guidance of the cells and movement is isotropic diffusion. Subsequently, no global organisation of the cell population occurs.

These simulations demonstrate the ability of a structured ECM to dictate and organise global cell movement patterns. Clearly, this may have important implications in, for example, the coordinated movements of early embryonic populations, the migratory pathways of immune cells or the directional spread of invasive tumours. The latter will be studied in greater detail in Section 5 while the former is expanded on in the discussion.

4 Rules for "mesenchymal" migration

4.1 Model rules

The simulations in Section 3 indicate a potentially crucial role of the ECM as a determinant of cell organisation. The absence of matrix remodelling, however, means the interaction is strictly one-way. The mesenchymal class of movement requires matrix remodelling by the cells, thereby introducing feedback between cells and their environment. In this section the modelling is extended to investigate the impact of this coupling on macroscopic cell organisation. The following generic rules define the model for "mesenchymal"-style migration:

(M1) contact guidance along matrix fibres,
(M2) slow cell speeds and infrequent turning,
(M3) extensive matrix remodelling.

The first two dictate the choice of cell movement turning functions and parameters: contact guidance has been demonstrated for a variety of cell types that adopt mesenchymal migration (e.g. Guido and Tranquillo 1993). To describe (M1) the same functional forms are employed as in Section 3, namely the turning function (4) is assumed in Equation 2. (M2) dictates speed and turning rates: except where stated the default values listed in Table 2 are employed. It is known that mesenchymal cells demonstrate a high degree of persistence in their direction of movement, however, as stated earlier, specific functional representation of this behaviour is not considered and its effect is absorbed into the mean turning rate.

Matrix remodelling comprises multiple processes, including degradation of fibres via proteolytic enzymes, the production and assembly of new matrix components and the rearrangement of fibres through mechanical forces. Studies from migrating carcinoma cells in 3D collagen gels have revealed the formation of "migration tracks": re-organised pathways along which the matrix fibres are aligned in the direction of cell migration (Friedl *et al.* 1997; Murphy and Gavrilovic 1999; Wolf *et al.* 2003b), see Figure 1. The functional role of these paths is unknown, however nearby cells have been observed to realign and move onto the trails, resulting in the formation of moving "cell-chains" (Friedl *et al.* 1997). It is currently unclear as to whether these are generated solely through the reshaping of the environment by the cells or whether direct cell-cell interactions are also required (e.g. through filopodial contacts or cell-cell adhesion). A use of the modelling here will be to study whether matrix remodelling and contact guidance are sufficient for the formation of the cell-chains.

Degradation of the ECM occurs through the action of proteolytic enzymes, such as MMPs, which can act in either a cell-localised or cell-nonlocalised manner. In the former, proteolytic enzymes are recruited to the membrane at the cell leading edge (Murphy and Gavrilovic 1999), thereby focusing proteolysis to the fore of the cell. In the latter, proteolytic enzymes are secreted into the environment as diffusible molecules, resulting in unfocused ECM destruction. The synthesis and assembly of new matrix components is essential in embryonic growth, maintaining the structure of healthy tissue and repairing wounded tissue. Matrix components are secreted into the extracellular space as individual collagen proteins by cells such as fibroblasts, where they assemble to form the long fibrils that characterise much of the ECM. Although it is possible for the individual collagen proteins to self organise into collagen fibres, cells themselves may play a significant role in their assembly (see Hay 1991).

Clearly, matrix remodelling is highly complex and the precise mechanisms involved will depend on both the cell type and the physiological context. Here, on the grounds of keeping the modelling both manageable and generic, three relatively simple sets of matrix dynamics are considered.

(R1) involves degradation of the matrix as a cell clears matrix fibres ahead of its migration path.

(R2) results in a constant macroscopic matrix density, but with locally realigned matrix fibres. This may be interpreted either as a process in which degraded matrix components are recycled and reincorporated into the matrix or as one in which cells rearrange the fibres through mechanical forces as they pass through it.

(R3) incorporates both matrix degradation and new matrix assembly and assumes these are independent. Cells are assumed to actively secrete matrix components and assemble them along their migration path. The dynamical difference to case (R2) is that the macroscopic matrix density will be altered as the cells pass through it according to the relative rates of matrix production and degradation.

4.1.1 Case R1

To set up appropriate equations to describe (R1), the remodelling forms proposed in Hillen (2006) are adapted. To illustrate this, consider the proteolytic action of a single cell as it migrates through the matrix. Rather than introduce extra complexity by incorporating additional variables, for example proteolytic enzymes, degradation is assumed to act at the the cell surface only and its action on the matrix is described phenomenologically. This assumption can be justified on the grounds that proteolytic enzymes are recruited to specific sites at the cell membrane. For a single cell, moving in direction θ and at position $\mathbf{x}$, the degradation rate of fibres with orientation ϕ is taken to be

$$-\delta\left(1-\psi\left|\cos(\theta-\phi)\right|\right) . \tag{6}$$

The matrix degradation parameter δ *in vivo/vitro* will depend on cell type, reaction rates in the degradation pathway, proteolytic enzyme concentrations *etc*, however here we simply take it to be constant. For varying $\psi \in [0,1]$ the above models either *focussed* or *unfocussed* proteolytic degradation. The former assumes that degrading proteins are recruited to the front of the cell. As such, cells are more likely to encounter and degrade those fibres orthogonal to their path, thus we set $\psi > 0$. For unfocussed proteolysis it is assumed cells have equal action on all matrix orientations.

To compute the overall degradation of the matrix, we sum over all cell orientations to derive type (R1) matrix dynamics:

$$m(\mathbf{x},\phi,t)_t = -\delta\left(\int_{-\pi}^{\pi}\left(1-\psi\left|\cos(\theta-\phi)\right|\right)c(\mathbf{x},\theta,t)d\theta\right)m(\mathbf{x},\phi,t)\,. \tag{R1}$$

Note that the above takes into account that cells migrating in opposite directions will have equivalent proteolytic action on the matrix.

4.1.2 Case (R2)

For (R2) matrix is remodelled but without alteration of the macroscopic density: as mentioned above, this may be interpreted either as a process in which fibres are redistributed during cell migration (for example, as a result of mechanical forces exerted by the cells on the matrix) or as a process in which the matrix components are recycled and reincorporated into the matrix. To derive the matrix dynamics, we consider the latter. Considering the modelling of proteolytic degradation above and integrating over all matrix directions, the sum total of matrix degraded at $\mathbf{x}$ will be

$$\delta\sigma = \delta\int_{-\pi}^{0}\left(\int_{-\pi}^{\pi}\left(1-\psi\left|\cos(\theta-\phi)\right|\right)c(\mathbf{x},\theta,t)d\theta\right)m(\mathbf{x},\phi,t)d\phi$$

To preserve the macroscopic matrix concentration, this matrix is reincorporated according to the existing matrix distribution. This leads to the type (R2) matrix dynamics:

$$m(\mathbf{x},\phi,t)_t = \delta\left(\sigma - \int_{-\pi}^{\pi}\left(1-\psi\left|\cos(\theta-\phi)\right|\right)c(\mathbf{x},\theta,t)d\theta\right)m(\mathbf{x},\phi,y) \tag{R2}$$

Note that this second form, coupled with the cell equation, is equivalent to that proposed in (Hillen (2006)).

4.1.3 Case R3

For the final form of matrix dynamics, it is assumed cells both degrade, produce and play an active role in assembling the matrix fibres as they migrate. Although matrix components such as collagen are capable of self-organising into fibres, *in vivo* the matrix proteins are generated intracellularly, transported to secretary sites localised to particular regions (e.g. the poles) of the cell surface and discharged into cell-controlled extracellular compartments where they are assembled into matrix fibres (Alberts *et al.* 1994; Hay 1991). The high level of regulation by the cell over this process allows matrix to be assembled in a controlled manner, for example, resulting in the construction of fibres along the path of cell migration.

We incorporate both matrix production and degradation into the model; here, these two processes are assumed to be independent, but *in vivo* they may well be linked internally or externally. Either way, the macroscopic matrix density may shift. Assuming that cells assemble the matrix fibres along their path then, coupled with the above modelling of proteolysis, we derive the following type (R3) dynamics:

$$m(\mathbf{x},\phi)_t = \delta\left(\gamma(c(\mathbf{x},\phi,t)+c(\mathbf{x},\phi+\pi,t)) - \left(\int_{-\pi}^{\pi}(1-\psi\left|\cos(\theta-\phi)\right|)\,c(\mathbf{x},\theta,t)d\theta\right)m(\mathbf{x},\phi)\right). \qquad \text{(R3)}$$

The above takes the bi-directional nature of the matrix into account through the assumption that matrix production depends on the sum $c(\mathbf{x},\phi,t)+c(\mathbf{x},\phi+\pi,t)$.

4.2 Numerics

The simulations from the amoeboid-style model in Figure 3 indicated that the ECM may play a significant role on the global organisation of motile cell populations through their tendency to follow matrix fibres. In the "mesenchymal-style" model, active feedback between cell movement and matrix remodelling takes place. In this section the impact of this feedback is investigated by simulating the transport model for the cells, Equation (1) with turning function (4) under the various forms for matrix dynamics given by (R1)–(R3).

4.2.1 Matrix dynamics

We first address how the different types of matrix dynamics (R1)–(R3) impact on its rearrangement. A population of cells migrating with fixed direction (i.e. $\mu = 0$) is placed in an initially nonoriented/random matrix (type (E1)). The initial location, final location and direction of cell movement is indicated in Figure 5 (a). Figure 5 (b) shows the alteration of the ECM under the various matrix dynamics for the following cases:

1. (R1) focussed degradation, $\psi = 1$ (Figure 5 (b1));
2. (R1) unfocussed degradation, $\psi = 0$ (Figure 5 (b2));
3. (R2) focussed remodelling, $\psi = 1$ (Figure 5 (b3));
4. (R3) focussed degradation with high matrix production, $\gamma = 5.0$, $\psi = 0.75$ (Figure 5 (b4));
5. (R3) focussed degradation with low matrix production, $\gamma = 0.5$, $\psi = 0.75$ (Figure 5 (b5)).

Other model parameters are taken at the default values listed in the "mesenchymal" column of Table 2.

For 1. matrix degradation occurs, but those fibres parallel to the cell migration path are left intact. The outcome is a trail of realigned matrix with lowered macroscopic matrix density (Figure 5 (b1)). A degree of realignment occurs for all values $\psi > 0$, however when $\psi = 0$ (case 2), corresponding to unfocussed degradation, all fibre orientations are altered equally resulting in a trail of almost completely cleared (yet unoriented) matrix (Figure 5 (b2)).

For 3. we expect a constant macroscopic matrix density following redistribution of the matrix fibres. This is confirmed in simulations (Figure 5 (b3)) whilst the matrix is redistributed such that it becomes aligned in the direction of cell movement. For 4. and 5., the amount of new matrix is independent of the amount degraded, resulting in a shift of the macroscopic matrix density following cell movement. The size of the shift will depend on the sizes of the parameters γ, δ *etc.*: in cases 4. and 5. (Figure 5 (b4) & (b5)) respectively an increase/decrease of the macroscopic matrix density is observed. The twin actions of focussed proteolytic action and assembly along the cell path results in an aligned matrix.

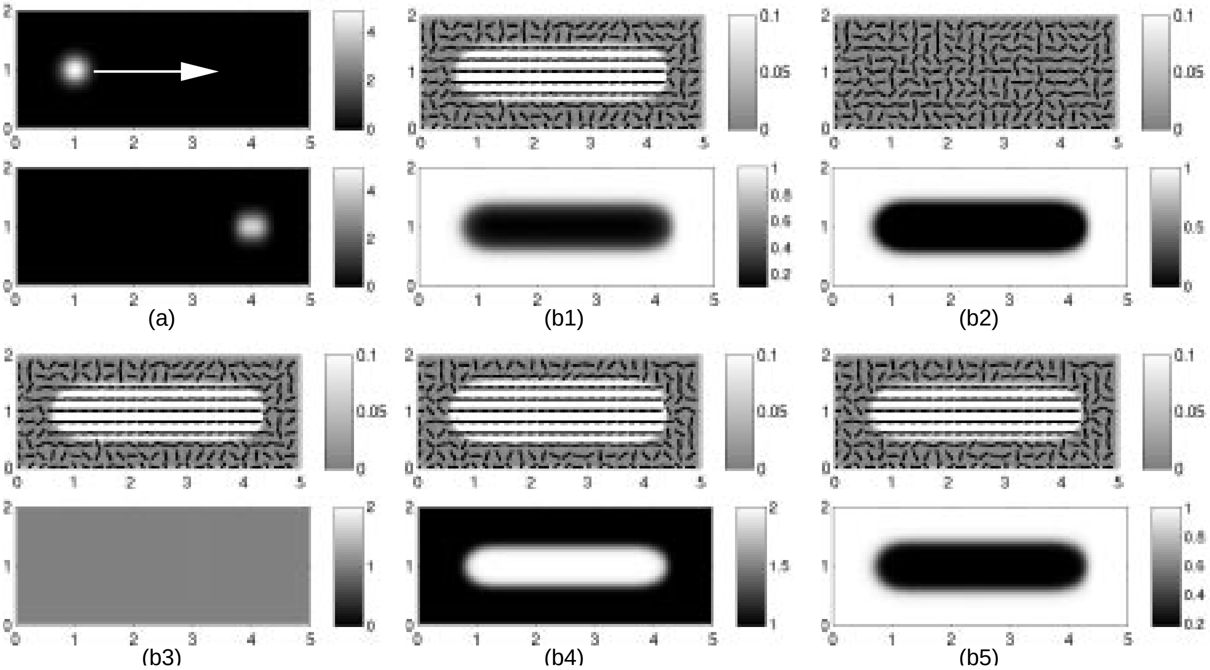

Fig. 5 Numerical solutions to explore ECM remodelling. (a) Macroscopic cell density at $t = 0$ and $t = 10$ hours. Cell population orientation indicated by arrow. (b1)-(b5) Distribution of matrix after 10 hours for each of cases 1.-5. in Section 4.2.1. Top row: Ψ (indicated by line orientation) and m_L (indicated by grayscale). Bottom row: $\overline{m}$. Numerical simulations employ parameter values as given in Table 2 (Mesenchymal column) except $\mu = 0$. Domain size $= 200 \times 500\ \mu\mathrm{m}^2$ using 40×100 spatial and 64 angular discretisation points. Scale: $1 = 100\mu$m.

4.2.2 Contact guidance and ECM remodelling

In this section the coupling between ECM remodelling and contact guided migration on the macroscopic cellular and matrix distributions is explored. For the rest of this section we restrict attention to matrix dynamics (R2) and (R3) since under (R1) matrix is destroyed to negligible levels. Evolution of the model is considered from an almost homogeneous initial distribution: cells are set at a small random perturbation about $1/2\pi$, normalised such that the macroscopic cell density $\overline{c} = 1$, while the matrix is set at type (E1) (i.e. random/unoriented).

The numerical simulations of the model are shown in Figure 6 (Movies showing the evolution of the cells and matrix can be found in the supplementary material). Simulations illustrate a process of macroscopic pattern formation during which cells become organised into long chains/networks underlain by pathways of aligned ECM. The mean length of the paths is significantly longer than the mean run length of the cells (defined as the speed/turning rate): for example, in the simulation displayed in Figure 6, paths on the order of several hundred μms are visible, as opposed to a mean run length of 10μm. An examination of the cell and matrix distributions at selected spatial points reveals additional information (Figure 7). For a dense cell chain, location 1 in Figure 6, the matrix is highly aligned in the direction of the cell path (Figure 7 (a), circles). The corresponding cell distribution reveals high cell densities moving in opposite directions along this path (Figure 7 (b), circles). On a lower density cell chain, location 2 in Figure 6, the matrix is less strongly aligned along the cell path (Figure 7 (a), triangles) and the corresponding cell distribution shows a much lower number of cells (Figure 7 (b)). Away from the cell chains, location 3 in Figure 6, the matrix is relatively unaligned and there is a very low cell density (Figure 7, stars). An extended simulation run time indicates these patterns persist: there is little difference between the patterns plotted after the first day and the patterns after 10 days (data not shown).

Further studies indicate that the twin actions of contact guidance and the realignment of the ECM by the cells are responsible for the formation of the networks: solutions when either $b = 0$ (zero contact

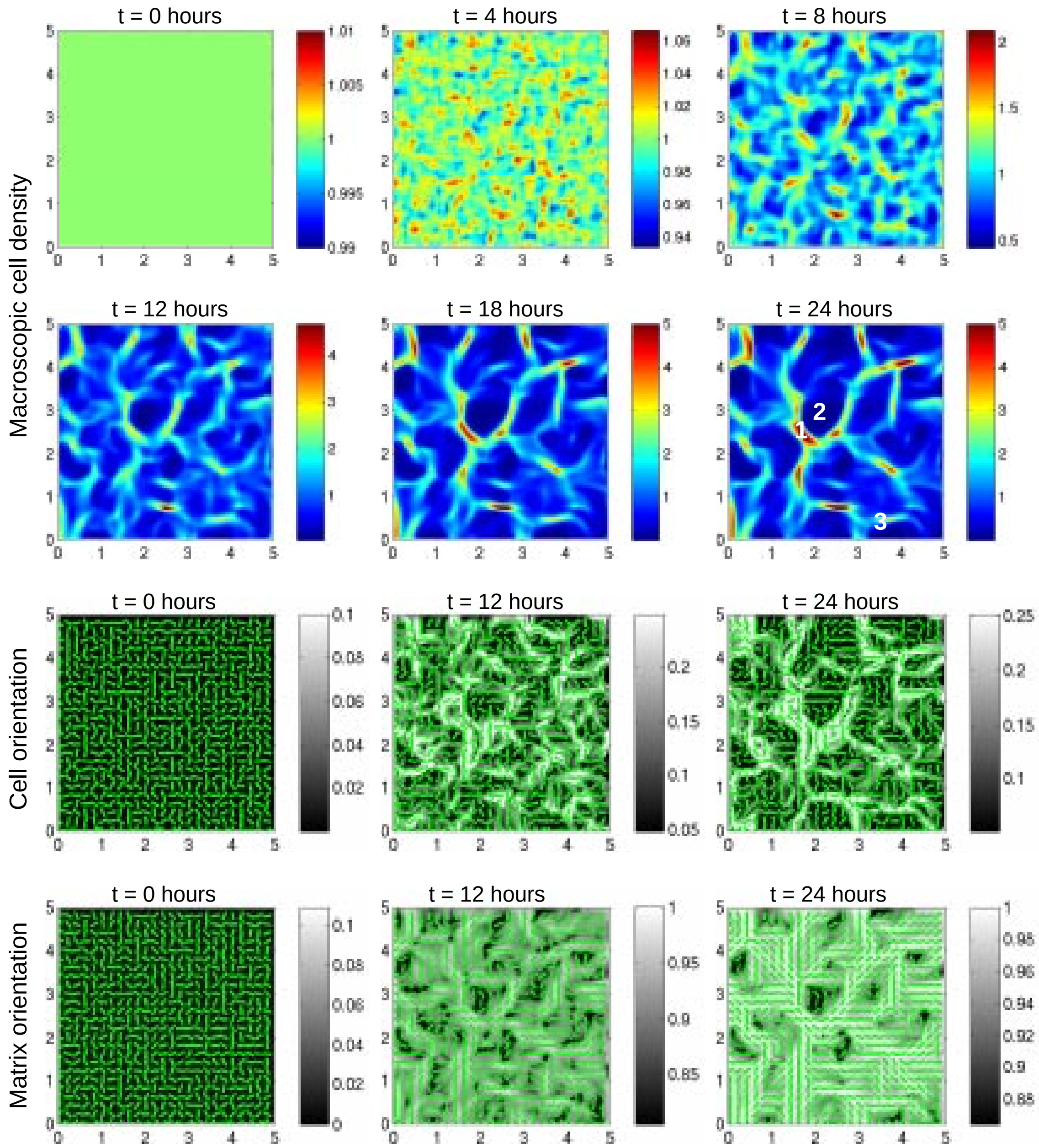

Fig. 6 Evolution of the transport model with (R2) matrix dynamics for focussed proteolysis ($\psi = 1$) and contact guidance ($b = 1$). Top two rows: macroscopic cell density $\overline{c}$. Third row: dominant cell orientation, Θ (green arrow) and strength of alignment c_L (grayscale). Fourth row: dominant matrix orientation, Φ (green line) and strength of alignment m_L (grayscale). Other parameters taken from Table 2 (mesenchymal column). Discretisation: 100×100 space and 64 angle points. Length scale $1 = 100\mu$m.

guidance) or $\psi = 0$ (no matrix realignment) fail to generate patterns and the cell/matrix distributions evolve to uniform distributions. Intermediate values of b and ψ allow networks to form, however these develop on a slower timescale. Simulations using different matrix dynamics (type (R3)) also indicates the possibility of chain formation, see Figure 8, thus indicating that patterning is not specific to a particular choice of kinetics. A detailed study into the conditions under which cell chain formation is possible will

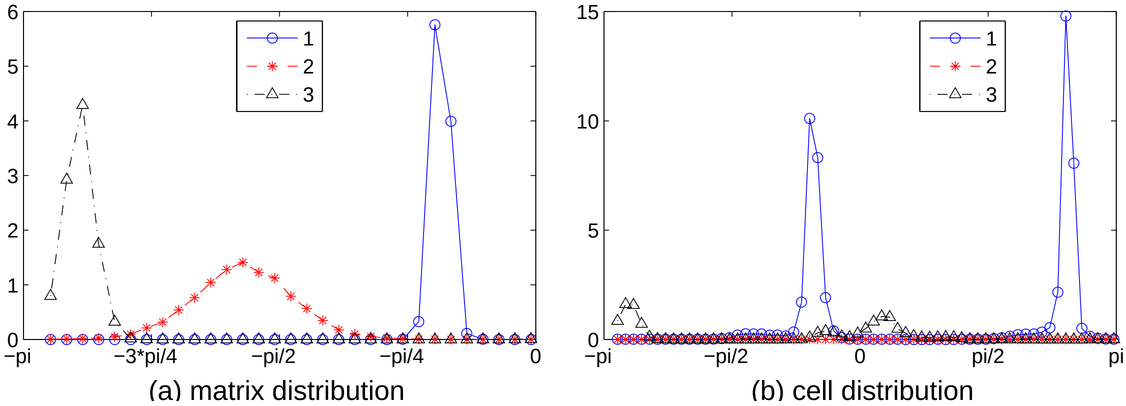

Fig. 7 Angular distributions of (a) matrix and (b) cells after $t = 24$ hours for the labelled positions 1, 2 and 3 in Figure 6.

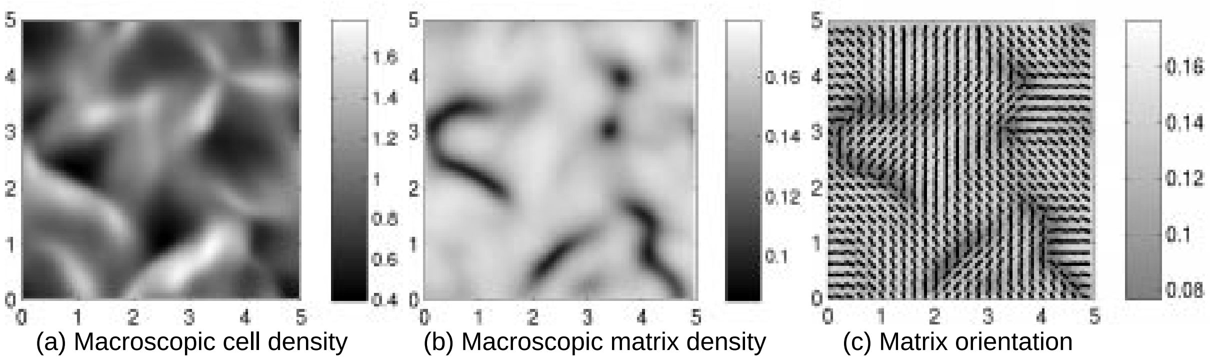

Fig. 8 Demonstrate of chain formation using (R3) matrix kinetics. Solutions plotted after 24 hours for parameters in Table 2 together with $\psi = 0.75$ and $\gamma = 0.5$. Length scale and discretisation details as in Figure 6.

be undertaken in future work, however the investigations reported here indicates the realignment of the matrix fibres in the path of cell migration is essential.

The simulations from the model suggest that the twin actions of matrix remodelling and contact guidance are sufficient for the generation of the network – there is no necessity for additional cell-cell interactions such as adhesion or filopodial contacts (although these may clearly play a further role in practice - note that a model incorporating the role of an aligned matrix, cell-cell interactions and chemotaxis has been developed in Chauviere *et al.* (2007)). The functional significance of the chains is unclear, yet as mentioned earlier they have been observed in both neural crest cell migration and in cancerous cell populations (Friedl *et al.* 1997; Kulesa and Fraser 1998; Jacques *et al.* 1998) and the creation of specific migration routes may allow more efficient shuttling of certain cell types. For example, the radial organisation of the matrix surrounding Peyer's patches in lymphoid tissues is consistent with the pathways of immune cells, however it is not clear the extent to which it is the cells themselves that have organised this matrix. The structure of the remodelled ECM displays a certain similarity to the ECM *in vivo* in tissues such as the dermis, where collagen fibres show a degree of local spatial organisation and structure with bundling and local alignment of the fibres (Imayama and Braverman 1989). Note that in the simulations here, the absence of specific guidance cues (for example, chemoattractants) results in a fairly random network structure.

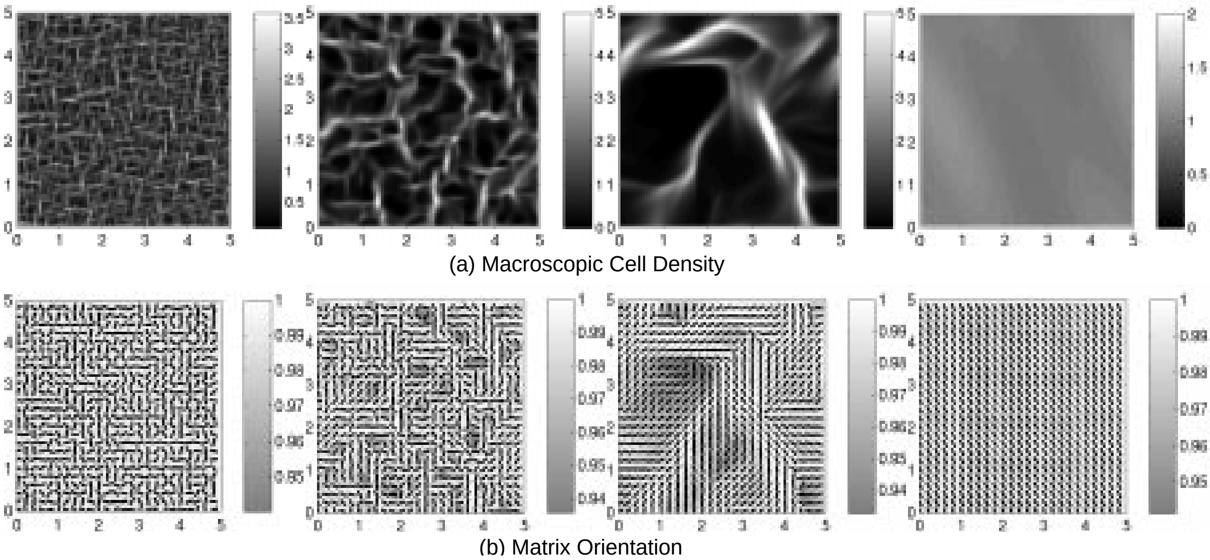

Fig. 9 Results from the parameter sensitivity analysis for alterations in the cell speed s_0 across two orders of magnitude. From left to right, $s_0 = 0.05, 0.25, 1.0$ and 5.0. Top row: macroscopic cell density ($\bar{c}$). Bottom row: matrix alignment (line: Φ, grayscale: m_L). Other parameters and discretisation data as in Figure 6. A similar set of results is obtained if the turning rate is appropriately altered.

4.2.3 Parameter sensitivity analysis

We tested the role of model parameters on the pattern forming capabilities of the model. As mentioned above, both focussed proteolysis and contact guidance are essential for the formation of the patterns (determined by setting either b or $\psi = 0$). We now investigate the effect of parameters s_0, μ and δ by considering a variation over two orders of magnitude range centred on the values in Table 2. Matrix dynamics are modelled using (R2) and we set $\psi = 1$. Alterations of either the speed, s_0, or the turning rate, μ, change properties of the moving cells and have a large impact on the structure of the trails (Figure 9). The effect of these two parameters can be linked together by considering the mean run length = speed/turning rate, corresponding to the average cell path length between reorientation. For a low mean run length (i.e. low cell speeds or high turning rates), chains are extremely short and the underlying ECM evolves with a high degree of spatial variation in its dominant orientation. As the mean run length increases, longer trails develop and the underlying ECM shows a greater degree of global organisation (i.e. the dominant local orientation of the matrix persists over a wide region of space). Increasing the mean run length further results in disappearance of chain formation and the ECM becomes globally oriented. Analytical investigations will be needed to further explore the relationship between the model parameters and the macroscopic patterning of the cells and matrix.

The parameter δ alters only the timescale of patterning: i.e. a small δ value corresponds to slow reorganisation of the matrix, and consequently slow formation of the chain patterns. A similar effect is observed on altering the initial macroscopic cell density: lower cellular densities still form patterns, but the development takes place over a longer timescale.

5 Application to tumour invasion

The acquired ability of tumour cells to break free from a tumour and invade surrounding tissue is a key event in its transformation to malignancy (Mareel and Leroy 2003). Invasion can occur in either an individual (amoeboid or mesenchymal) or collective manner (Friedl and Wolf 2003) according to cancer type and origin and can result in complex and heterogeneous patterns of invasion, for example “fingering” patterns (strands of cells extending out from the main tumour mass), “nesting”, cell-chains or individual isolated cells. Enormous effort has been invested into understanding the interplay between the invading cancer cells and the host tissue (e.g. see Mareel and Leroy 2003), research that has spawned a large number of mathematical models for cancer invasion (for a review, see Araujo and McElwain 2004).

A number of these models (e.g. Perumpanani and Byrne 1999; Perumpanani *et al.* 1998; Anderson *et al.* 2000; MacArthur *et al.* 2005; Chaplain and Lolas 2005) have focussed on the role played by the ECM in providing a substrate for the binding of adhesive molecules and cell movement. Tumour cells follow gradients in these molecules (a process known as haptotaxis) and the modelling has provided critical information into, for example, the effect of matrix density on the rate of cancer invasion. The precise organisation/architecture of the ECM and its impact has generally been neglected in models for cancer invasion. Here, an exploration of this issue is initiated.

The model is formulated in a simple and generic way (i.e. there is no specific tumour/tissue environment), although an inherent assumption is that migration takes place via one of the individual migration strategies (amoeboid/mesenchymal) described earlier. Where applicable, type (R2) matrix dynamics are assumed, thereby assuring a constant macroscopic matrix density. Of course, in reality both the matrix alignment and density may undergo significant change, according to tissue and cancer origin, with a correspondingly large impact on tumour infiltration. The assumption of (R2) dynamics allows attention to be focussed solely on the role of matrix alignment. Future extensions of the model will incorporate additional factors such as the impact of matrix density, adhesion receptors bound to the ECM *etc.*.

In the modelling that follows the set-up illustrated in Figure 10 (a) is considered. An initially tumour free ECM region is assumed to be bordered on one side ($x = 0$) by a compact solid tumour ($x < 0$). It is presumed that the tumour was previously non-invasive, however from $t = 0$ a steady flow of tumour cells escapes the main tumour mass and invades the surrounding ECM. An interpretation for this would be a mutation arising in the main tumour mass leading to down-regulation in cell-cell adhesion and subsequent escape into the ECM. To focus only on the invasion process, cell kinetics are currently ignored – i.e. migrating cells do not proliferate. For the timeframe considered in the numerical simulations, this is a reasonable approximation.

It is assumed that, as before, cells move through contact guidance and we therefore simulate Equation (1) with turning function (4). Rather than consider a single form for the cell velocity, the following two cases are considered:

$$\mathbf{v}(\mathbf{x},\theta) = s_0(\cos\theta, \sin\theta) \quad \text{or} \quad \mathbf{v}(\mathbf{x},\theta) = \begin{cases} s_0 \frac{m(\mathbf{x},\theta)}{\overline{m}(\mathbf{x})}(\cos\theta, \sin\theta) & \text{if} \quad \theta \in (-\pi, 0] \\ s_0 \frac{m(\mathbf{x},\theta-\pi)}{\overline{m}(\mathbf{x})}(\cos\theta, \sin\theta) & \text{if} \quad \theta \in (0, \pi] \end{cases}$$

which we term *constant* and *alignment-dependent* respectively. The latter form assumes cell velocity increases with the strength of alignment. While this is somewhat speculative in nature, an intuitive explanation is that cells migrating in an aligned matrix may need to spend less time circumnavigating obstacles or clearing the matrix.

The boundary conditions for the cells require special attention and are described as follows. Along the left and right boundaries we consider periodic boundary conditions. To model the invasion process we assume that along $x = 0$ there is a positive flux of upward-moving invasive cells crossing into the ECM region. This flux is assumed to be uniform across the tumour-ECM border. Cells moving downwards across $x = 0$ are assumed to be deflected due to the presence of the solid tumour, and reverse their migratory direction. Along $x = L_x$ we assume that any cells moving upwards "escape" and do not re-enter (i.e. there is a flux out of the domain resulting from cells moving "upwards" across $x = L_x$) and zero-flux "downwards" across $x = L_x$.

5.1 Amoeboid/negligible-ECM remodelling

In the first set of simulations it is assumed cell movement is of "amoeboid"-style, i.e. contact-guided migration occurs but without any ECM remodelling. The focus is on how the structure of the matrix alters the pattern of invasive spread. To this end, the 4 matrix types displayed in Figure 10 (b) are considered: a *random* matrix with no dominant alignment, a globally oriented ECM aligned *parallel* to the tumour-ECM boundary, a globally oriented ECM aligned *orthogonal* to the tumour-ECM boundary and a *mixed* scenario.

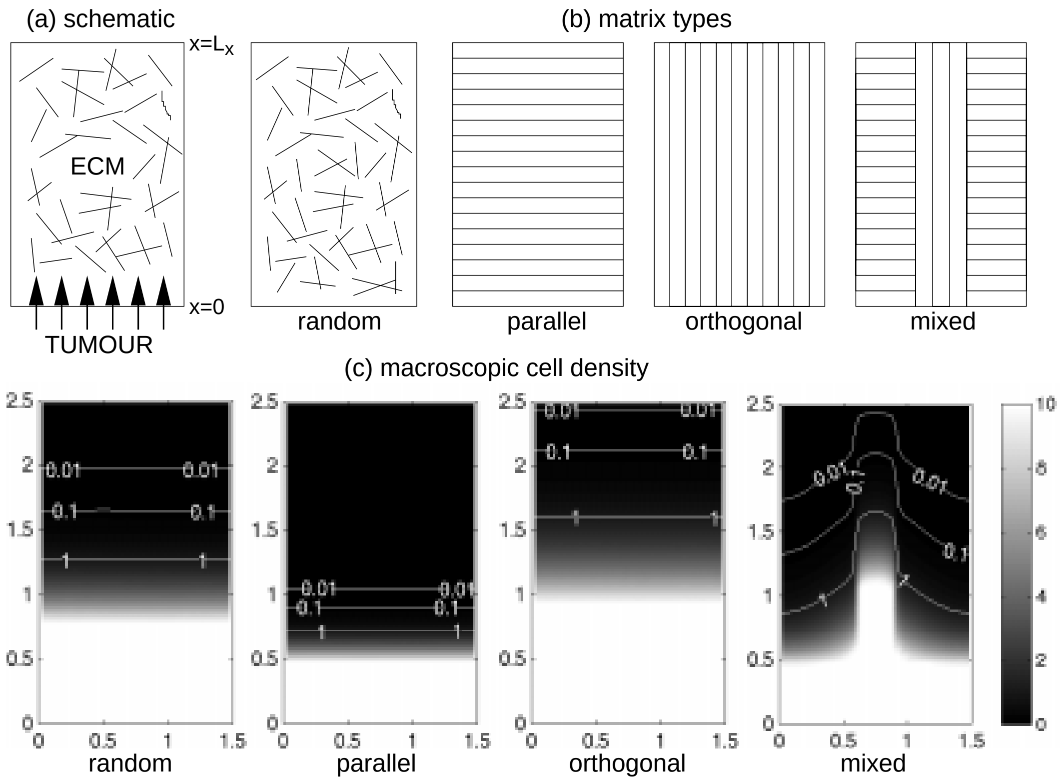

Fig. 10 (a) Schematic showing the set-up in the model for tumour invasion. (b) The four underlying ECM types. (c) Simulation result showing the macroscopic cell density for amoeboid migration following 8 hours of simulation time for constant cell speed $s_0 = 2.5\mu$m/min and $\mu = 1.0$/min on a spatial grid of dimensions 250×150 μm^2.

Figure 10 (c) displays the results of the numerics following 8 hours using the constant velocity (with $s_0 = 2.5\mu$m/min and $\mu = 1.0$/min). As can clearly be seen from the numerics, the structure of the ECM may have a significant effect on the infiltration rate into healthy tissue: in relation to the "random" ECM, the "orthogonally"-oriented ECM permits much faster invasion while the "parallel"-oriented ECM permits much slower invasion. For more complicated ECM structures, such as the "mixed" type represented in Figure 10 (b), the invasion pattern may be complex with a heterogeneous pattern of tissue invasion. This suggests that invasive tumours originating in highly structured matrix may show a complex pattern of infiltration. This is expanded on further in Section 5.3.

5.2 Mesenchymal/ECM remodelling

Reorganisation of the ECM is now incorporated by assuming the invading cells adopt a mesenchymal class of movement. As stressed above, the macroscopic matrix density is assumed constant (type (R2) dynamics with $\psi = 1$). For the simulations here, an initially nonoriented/random ECM is considered (type (E1)). With a uniform rate of invasion along the tumour-ECM border and a nonoriented ECM, the invasion rate is almost uniform with y and 2D data is thus represented by plotting of the macroscopic cell density ($\overline{c}$) and strength of matrix alignment (m_L) as a function of x only (representing the depth of invasion).

With the incorporation of matrix remodelling, the matrix remodelling rate δ becomes a critical parameter. In Figure 11 (a) invasion profiles are plotted for varying values of δ and a constant cell migration speed following 8 hours of simulation time. An increase in δ results in only marginal increase in the degree of invasion (top row). However, the matrix shows an increased level of alignment (with fibres aligned in the direction of cell invasion) behind the invasion wavefront (bottom row).

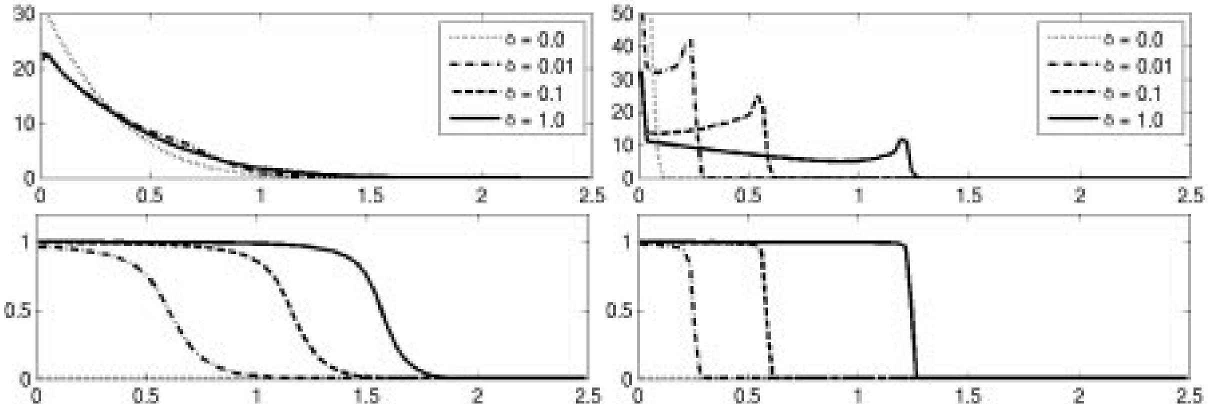

Fig. 11 Tumour invasion with ECM remodelling. Top row: Macroscopic cell density ($\overline{m}$), bottom row: strength of matrix alignment (m_L). (a) Constant cell speed with $s_0 = 0.5\mu$m/min and $\mu = 0.05$/min (b) Alignment-dependent cell speed with $s_0 = 1.0\mu$m/min. Equations solved on a spatial grid of dimensions 250×150 μm^2.

Under an alignment-dependent cell speed, the extent of cell invasion is strongly dependent on the matrix remodelling rate, Figure 11 (b). With negligible matrix remodelling, very little invasion takes place as cells remain "trapped" near the tumour-ECM border. As δ is increased, however, the realignment of the matrix in the direction of cell invasion results in a dramatic increase in the depth of invasion. The cell density profile now has a compact wavefront with cells "stacking" at the tip of invasion. Intuitively, the compact form of the tumour derives from invading cells migrating quickly across the aligned ECM region before accumulating on reaching the unorganised ECM.

5.3 Invasion into a remodelled matrix

In the final simulation from this preliminary investigation, the effect of tumour invasion into a previously remodelled matrix is considered. As mentioned earlier, the ECM derived following mesenchymal movement displays a certain similarity to the structure of ECM *in vivo* in tissues such as the dermis. A simulation is conducted to investigate invasion into remodelled ECM derived from the simulation in Figure 6. The numerical results are displayed in Figure 12 for (a) amoeboid, and (b) mesenchymal migration, however a direct comparison between the two cases is somewhat redundant due to different choices of parameters such as the cell speed. In both cases, a constant cell velocity was considered.

The numerics for both types of invasion reveal a complex and spatially heterogeneous pattern of tumour infiltration. The aligned and spatially varying structure of the matrix results in enhanced migration along specific pathways, yielding a macroscopic fingering process. For amoeboid migration, no matrix remodelling occurs and therefore the matrix structure displayed after 24 hours is the same as its initial distribution. For mesenchymal migration, the matrix is remodelled, however only in a manner to reinforce the existing orientational structure of the matrix.

These simulations serve to reinforce the notion that matrix structure and organisation may strongly impact on the type of tumour invasion. Complex patterns of tumour invasion, for example "fingering" and cell-chain invasion may arise solely as a result of the cell-matrix interactions.

6 Discussion

In this paper a continuous transport model has been developed to understand the role of a structured extracellular matrix on the collective organisation of migrating cell populations. Continuous transport equations have frequently been described in the literature as "mesoscopic": they provide a bridge between a truly "microscopic" approach in which each cell is modelled as a discrete/individual object with precise

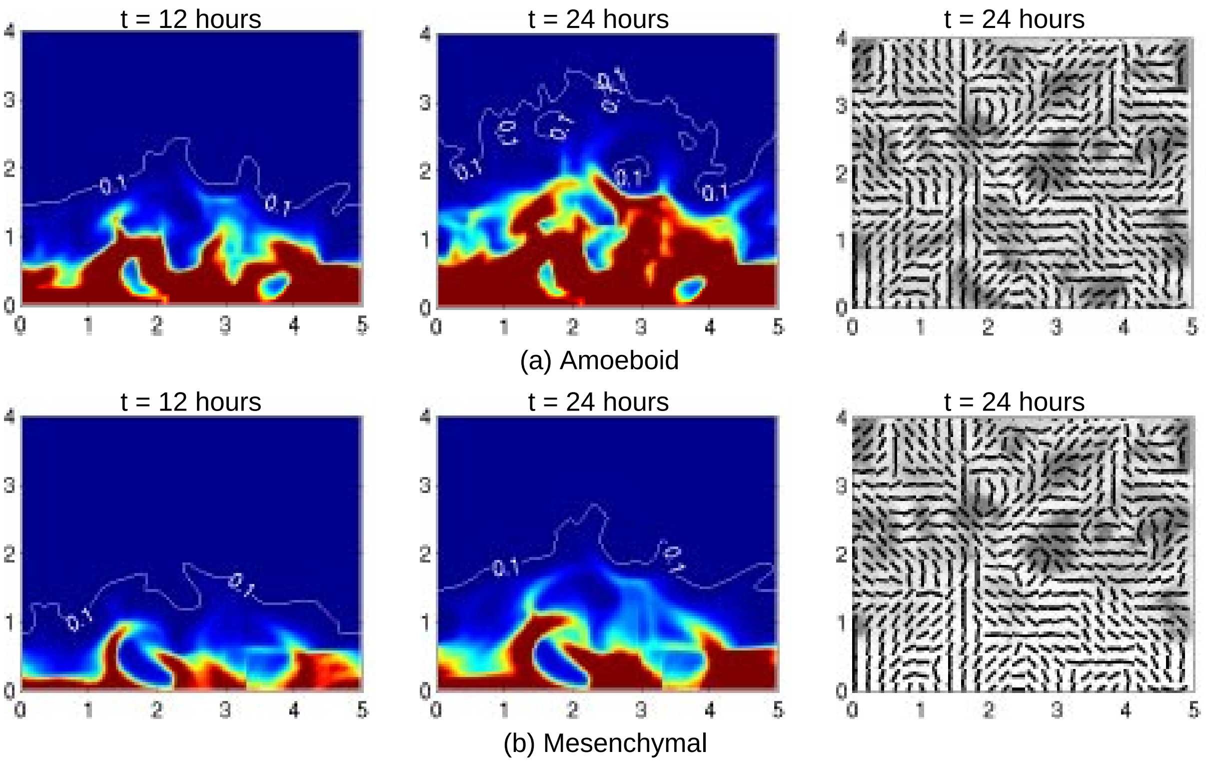

Fig. 12 Tumour invasion into a previously remodelled ECM. (a) Amoeboid migration with $s_0 = 2.5\mu$m/min, $\mu = 1.0$/min. (b) Mesenchymal migration with $s_0 = 0.5\mu$m/min, and $\mu = 0.05$/min and $\delta = 0.1$. The initial matrix distribution was taken from Figure 6 and as indicated by the top right plot. Discretisation details as in Figure 6.

rules for movement and a "macroscopic" model based on evolution equations for variables such as the macroscopic cell/matrix densities in which movement is modelled in terms of a total population flux. The transport model retains a microscopic description of cell movement yet provides illumination on the dynamics of macroscopic variables. Weighed against these advantages, however, they are comparatively more taxing to solve numerically or analytically than a macroscopic approach.

The model here can be solved in a multiscale manner: a discrete model may be developed to describe the underlying velocity-jump model upon which the transport equation is based and utilised in situations where the cell density is low or more complex models for cell behaviour required. Preliminary simulations of a discrete formulation of the model presented here indicates a close correspondence with the behaviour of the continuous transport model. The continuous transport model may be used to understand the dynamics of systems where the number of cells is unfeasibly large for a discrete approach or when a greater understanding of the macroscopic properties of the system are required. Through appropriate scaling of the length and time scales, it is possible to derive a fully macroscopic model for the cell density to tackle large scale biological processes (Hillen 2006). An important area under current investigation is to determine whether the "cell-chain" behaviour reported here can also be observed in its corresponding macroscopic model. The connection between microscopic/mesoscopic models of movement and their macroscopic counterparts is an important area which has received little rigorous treatment, although some work has been initiated for a "space-jump" type model of movement (Painter *et al.* 2003; Horstmann *et al.* 2004).

In the "amoeboid" model simulations it was shown how the ECM structure can organise cells, for example inducing colocalisation despite the non-directional nature of the matrix fibres and the absence of other environmental cues (e.g. adhesion gradients, chemotactic cues). These results echo experimental observations of motile cells placed on micro-fabricated structures (Wood 1988) and support the notion that the architecture of the ECM may play an important role in the organisation of cell populations during embryonic growth or facilitating movement during physiological processes. Ultrastructural studies of the developing pectoral fin in fish indicates contact guidance may play an important role directing cell movement (Wood and Thorogood 1984; Thorogood and Wood 1987): a potential application of the model here would be to test whether the ECM alone is capable of directing these cell movement patterns, or if additional environmental cues (for example, chemoattractants) are required. Contact guidance has also been suggested as playing a role in the *in vivo* guidance of early embryonic neural crest cells, (Newgreen 1989) and in the guidance of adult lymphocytes. Detailed studies of "Peyer's-patches" in the mouse indicate a radial pattern of ECM fibre alignment consistent with the migration pathways of lymphocyte cells in and out of the patch (Ohtsuka *et al.* 1992). Clearly, contact guided migration may play a role in facilitating the speed and guidance of the lymphocyte cells.

In the simulations of mesenchymal migration, we demonstrated the macroscopic formation of networks or cell-chains: dense connected pathways of motile cells similar to those reported in a number of *in vitro* and *in vivo* systems, including tumour cells (Friedl *et al.* 1997), neural crest cells (Kulesa and Fraser 1998) and glioma gel assays (Kaufman *et al.* 2005). The modelling here indicates that the twin actions of contact-guided migration along ECM fibres and an ECM remodelling process in which fibres become aligned along the path of cell migration are sufficient conditions for this process to occur — thus it is not necessary for additional interactions to take place, such as the formation of adhesive interactions between cells, cell-contact through filopodial interactions or communication via chemoatrractants, although clearly all such processes may play a role in *in vivo* examples of chain formation. A clear area for future work would be analytical investigation into the conditions for which network patterns arise and their structure. The resemblance of the remodelled ECM to *in vivo* matrix in tissues such as the dermis indicate an ongoing process of cellular migration (for example, as a result of normal tissue repair, immune systems response) may result in gradual reorganisation of the skin.

One significant extension is to model dermal wound healing. In the early stages of healing, fibroblasts migrate into the wounded region to regenerate the ECM through secretion and assembly of collagen and other matrix components. Scarred tissue shows a significantly greater degree of bundling and alignment of the fibres than normal tissue, resulting in its different appearance and weaker nature. A variety of models have been developed by Sherratt and others (e.g. Dallon *et al.* 1999, 2001; McDougall *et al.* 2006; Olsen *et al.* 1998, 1999; Dallon and Sherratt 1998, 2000) to determine the role of biological parameters on the form of the reconstituted matrix. The patterning and the matrix structure from the mesenchymal simulations here echo their results: for example, we demonstrated that the spatial scale of the "globally aligned regions" (see Figure 9) depended on cell parameters such as speed and turning rates. It would be of interest to extend the modelling here to further compare the results to obtain new insights into the mechanistic basis of wound healing.

The cell chain patterns presented here display a striking similarity to the network of endothelial cells formed during "vasculogenesis", the early embryonic formation of the vasculature. Vasculogenesis is a multi-step process in which endothelial cells first form a connected network structure through their response to chemical signals (principally VEGF) and the surrounding ECM before undergoing tubularisation to form the blood capillaries. A great deal of understanding of this process has derived from *in vitro* models in which cells are cultivated in a "Matrigel" scaffold. A number of mechanochemical models have been developed that incorporate the mechanical forces between the endothelial cells and the surrounding matrix (for example, see the reviews in Chapter 8 of Murray (2003) and Ambrosi *et al.* (2005) for more information). The model developed here suggests that the twin actions of focussed proteolysis by the cells and contact guidance migration may be sufficient in generating the early network patterns, however it is important to note that the model here neglects the forces between the cells and the matrix that will undoubtedly play a role in the patterning process. Omission of these details suited the purposes of the current modelling, where a simpler and more phenomenological model was desirable, however an important future extension of the model should be a more realistic description for the mechanical forces acting between cells and the matrix.

Preliminary simulations have been conducted to understand how the matrix organisation may impact on the rate and pattern of tumour invasion. Whilst the model was purposefully kept simple in nature, it implied that the orientational structure of the ECM could be a significant determinant on the rate and heterogeneity of tumour invasion. Significantly, we demonstrated that invasion into a complex ECM environment could, through the simple action of matrix fibre following, give rise to complex "fingering" types of tumour invasion. These results indicate that for highly structured connective tissues (such as the bone and dermis), clear understanding of the nature of the matrix may assist in identifying pathways of invasion. Another potential application for extension of the modelling lies in describing the growth pattern of gliomas. The heterogeneous growth of these brain tumours are believed to stem from regional variability in the environment (Swanson *et al.* 2002). For example, the rapid spread across the *corpus callosum* has been attributed to the tendency of individual glioma cells to migrate along the highly aligned white matter tracts (Bellail *et al.* 2004). Macroscopic models of glioma growth have been formulated utilising an anisotropic diffusion tensor (Clatz *et al.* 2005) derived from Diffusion Tensor Imaging (DTI) data that indicates the white matter tract anatomy (Price *et al.* 2003). Significantly, the fully macroscopic models derived from an underlying description of contact-guided cell migration along ECM fibres (Hillen 2006) comprise of a PDE equation incorporating an anisotropic diffusion tensor based on the underlying extracellular architecture. The modelling can thus potentially implicate a link between a guided individual cell migration of cells along white matter fibre tracts and the global patterns of glioma spread.

Incorporating remodelling of the matrix into the model demonstrated the importance of understanding how cell migration parameters (such as cell speed) depend on the alignment structure of the matrix. Under reasonable assumptions for the cell speed, large variations in the degree of invasion could be observed. Clearly, this latter work may be extended in a number of manners. For example, a more precise incorporation of the manner in which cells remodel the matrix, inclusion of long range proteolytic enzymes, the role of adhesion molecules in the matrix and other chemical factors should all be considered in the modelling. This will form part of future extensions of the modelling.

Acknowledgements. The author would like to express his gratitude to Thomas Hillen, who has provided the stimulant for much of this work as well as a number of highly constructive suggestions. The author would further like to thank the two anonymous referees for their helpful comments. This work has been partially supported by an NIH grant CA113004.

References

Alberts, B., Bray, D., Lewis, J., Raff, M., Roberts, K., and Watson, J. (1994). *Molecular Biology of the Cell*. Garland Publishing Inc., New York, London.

Ambrosi, D., Bussolino, F., and Preziosi, L. (2005). A review of vasculogenesis models. *J. Theor. Med.*, **6**, 1–19.

Anderson, A. R. A., Chaplain, M., Newman, E., Steele, R., and Thompson, E. (2000). Mathematical modelling of tumour invasion and metastasis. *J. Theor. Med.*, **2**, 129–153.

Araujo, R. P. and McElwain, D. L. S. (2004). A history of the study of solid tumour growth: the contribution of mathematical modelling. *Bull. Math. Biol.*, **66**, 1039–1091.

Barocas, V. and Tranquillo, R. (1997). An anisotropic biphasic theory of tissue-equivalent mechanics: The interplay among cell traction, fibrillar network deformation , fibril alignment and cell contact guidance. *J. Biomechanical Eng.*, **119**, 137–145.

Bellail, A. C., Hunter, S. B., Brat, D. J., Tan, C., and Van Meir, E. G. (2004). Microregional extracellular matrix heterogeneity in brain modulates glioma cell invasion. *Int. J. Biochem. Cell. Biol.*, **36**, 1046–1069.

Chaplain, M. and Lolas, G. (2005). Mathematical modelling of cancer cell invasion of tissue: the role of the urokinase plasminogen activation system. *Math. Models and Meth. in Appl. Sci.*, **15**, 1685–1734.

Chauviere, A., Hillen, T., and Preziosi, L. (2007). Modeling cell movement in anisotropic and heterogeneous network tissues. *Networks and Heterogeneous Media*, **2**, 333–357.

Clatz, O., Sermesant, M., Bondiau, P., Delingette, H., Warfield, S., Malandain, G., and Ayache, N. (2005). Realistic simulation of the 3d growth of brain tumours in mr images coupling diffusion with biomechanical deformation. *IEEE Trans. Med. Imag.*, **24**, 1334–1345.

Dallon, J. and Sherratt, J. (2000). A mathematical model for spatially varying extracellular matrix alignment. *SIAM J. Appl. Math.*, **61**, 506–527.

Dallon, J. C. and Sherratt, J. A. (1998). A mathematical model for fibroblast and collagen orientation. *Bull. Math. Biol.*, **60**, 101–129.

Dallon, J. C., Sherratt, J. A., and Maini, P. K. (1999). Mathematical modelling of extracellular matrix dynamics using discrete cells: fiber orientation and tissue regeneration. *J. Theor. Biol.*, **199**, 449–471.

Dallon, J. C., Sherratt, J. A., and Maini, P. K. (2001). Modeling the effects of transforming growth factor-beta on extracellular matrix alignment in dermal wound repair. *Wound Repair. Regen.*, **9**, 278–286.

Dickinson, R. (1997). A model for cell migration by contact guidance. In W. Alt, A. Deutsch, and D. G., editors, *Dynamics of Cell and Tissue Motion*, pages 149–158, Basel. Birkhauser.

Dickinson, R. (2000). A generalized transport model for biased cell migration in an anisotropic environment. *J. Math. Biol.*, **40**, 97–135.

Dunn, G. A. and Heath, J. P. (1976). A new hypothesis of contact guidance in tissue cells. *Exp. Cell Res.*, **101**, 1–14.

Francis, K., Palsson, B., Donahue, J., Fong, S., and Carrier, E. (2002). Murine Sca-1(+)/Lin(-) cells and human KG1a cells exhibit multiple pseudopod morphologies during migration. *Exp. Hematol.*, **30**, 460–463.

Friedl, P. (2004). Prespecification and plasticity: shifting mechanisms of cell migration. *Curr. Opin. Cell. Biol.*, **16**, 14–23.

Friedl, P. and Wolf, K. (2003). Tumour-cell invasion and migration: diversity and escape mechanisms. *Nat. Rev. Cancer*, **3**, 362–374.

Friedl, P., Maaser, K., Klein, C. E., Niggemann, B., Krohne, G., and Zanker, K. S. (1997). Migration of highly aggressive MV3 melanoma cells in 3-dimensional collagen lattices results in local matrix reorganization and shedding of alpha2 and beta1 integrins and CD44. *Cancer Res.*, **57**, 2061–2070.

Friedl, P., Zanker, K. S., and Brocker, E. B. (1998). Cell migration strategies in 3-D extracellular matrix: differences in morphology, cell matrix interactions, and integrin function. *Microsc. Res. Tech.*, **43**, 369–378.

Gaudet, C., Marganski, W. A., Kim, S., Brown, C. T., Gunderia, V., Dembo, M., and Wong, J. Y. (2003). Influence of type I collagen surface density on fibroblast spreading, motility, and contractility. *Biophys. J.*, **85**, 3329–3335.

Gerisch, A. and Chaplain, M. (2007). Mathematical modelling of cancer cell invasion of tissue: local and non-local models and the effect of adhesion. *J. Theor. Biol.*, page doi:10.1016/j.jtbi.2007.10.026.

Guido, S. and Tranquillo, R. T. (1993). A methodology for the systematic and quantitative study of cell contact guidance in oriented collagen gels. Correlation of fibroblast orientation and gel birefringence. *J. Cell. Sci.*, **105**, 317–331.

Hay, E., editor (1991). *Cell Biology of Extracellular Matrix*. Plenum Press, New York, 2nd edition.

Hillen, T. (2002). Hyperbolic models for chemosensitive movement. *Math. Models and Methods in Appl. Sci.*, **12**, 1007–1034.

Hillen, T. (2006). M^5 mesoscopic and macroscopic models for mesenchymal motion. *J. Math. Biol.*, **53**, 585–616.

Horstmann, D., Painter, K., and Othmer, H. (2004). Aggregation under local reinforcement: from lattice to continuum. *Eur. J. Appl. Math.*, **15**, 545–576.

Hughes, L., Archer, C., and Gwynn, A. (2005). The ultrastructure of mouse articular cartilage: collagen orientation and implications for tissue functionality. a polarised light and scanning electron microscope study and review. *Eur. Cells. and Mat.*, **9**, 68–84.

Imayama, S. and Braverman, I. M. (1989). A hypothetical explanation for the aging of skin. Chronologic alteration of the three-dimensional arrangement of collagen and elastic fibers in connective tissue. *Am. J. Pathol.*, **134**, 1019–1025.

Jacques, T. S., Relvas, J. B., Nishimura, S., Pytela, R., Edwards, G. M., Streuli, C. H., and ffrench Constant, C. (1998). Neural precursor cell chain migration and division are regulated through different beta1 integrins. *Development*, **125**, 3167–3177.

Kaufman, L. J., Brangwynne, C. P., Kasza, K. E., Filippidi, E., Gordon, V. D .and Deisboeck, T. S., and Weitz, D. A. (2005). Glioma expansion in collagen I matrices: analyzing collagen concentration-dependent growth and motility patterns. *Biophys. J.*, **89**, 635–650.

Kulesa, P. M. and Fraser, S. E. (1998). Neural crest cell dynamics revealed by time-lapse video microscopy of whole embryo chick explant cultures. *Dev. Biol.*, **204**, 327–344.

Lauffenburger, D. A. and Horwitz, A. F. (1996). Cell migration: a physically integrated molecular process. *Cell*, **84**, 359–369.

Locascio, A. and Nieto, M. A. (2001). Cell movements during vertebrate development: integrated tissue behaviour versus individual cell migration. *Curr. Opin. Genet. Dev.*, **11**, 464–469.

MacArthur, B. D., Please, C. P., and Pettet, G. J. (2005). A mathematical model of dynamic glioma-host interactions: receptor-mediated invasion and local proteolysis. *Math. Med. Biol.*, **22**, 247–264.

Mareel, M. and Leroy, A. (2003). Clinical, cellular, and molecular aspects of cancer invasion. *Physiol. Rev.*, **83**, 337–376.

McDougall, S., Dallon, J., Sherratt, J., and Maini, P. (2006). Fibroblast migration and collagen deposition during dermal wound healing: mathematical modelling and clinical implications. *Phil. Trans. R. Soc. Lond. A*, **364**, 1385–1405.

Mogilner, A. and Edelstein-Keshet, L. (1996). Spatio-angular order in populations of self-aligning objects: formation of oriented patches. *Physica D*, **89**, 346–367.

Mogilner, A., Edelstein-Keshet, L., and Ermentrout, G. (1996). Selecting a common direction. ii. peak-like solutions representing total alignment of cell clusters. *J. Math. Biol.*, **34**, 811–842.

Murphy, G. and Gavrilovic, J. (1999). Proteolysis and cell migration: creating a path? *Curr. Opin. Cell. Biol.*, **11**, 614–621.

Murray, J. (2003). *Mathematical Biology II: Spatial models and biochemical applications*. Springer, New York, 3rd edition.

Newgreen, D. F. (1989). Physical influences on neural crest cell migration in avian embryos: contact guidance and spatial restriction. *Dev. Biol.*, **131**, 136–148.

Ohtsuka, A., Piazza, A. J., Ermak, T. H., and Owen, R. L. (1992). Correlation of extracellular matrix components with the cytoarchitecture of mouse Peyer's patches. *Cell Tissue Res.*, **269**, 403–410.

Olsen, L., Maini, P., Sherratt, J., and Marchant, B. (1998). Simple modelling of extracellular matrix alignment in dermal wound healing. *J. Theor. Med*, **1**, 172–192.

Olsen, L., Maini, P., Sherratt, J., and Dallon, J. (1999). Mathematical modelling of anisotropy in fibrous connective tissue. *Math. Biosci.*, **158**, 145–170.

Othmer, H., Dunbar, S., and Alt, W. (1988). Models of dispersal in biological systems. *J. Math. Biol.*, **26**, 263–298.

Painter, K., Horstmann, D., and Othmer, H. (2003). Localization in lattice and continuum models of reinforced random walks. *Appl. Math Lett.*, **16**, 375–381.

Perumpanani, A., Simmons, D., Gearing, A., Miller, K., Ward, G., Norbury, J., Schneemann, M., and Sherratt, J. (1998). Does extracellular matrix mediated chemotaxis promote or impede cell migration? *Proc. R. Soc. Lond. B*, **265**, 2347–2352.

Perumpanani, A. J. and Byrne, H. M. (1999). Extracellular matrix concentration exerts selection pressure on invasive cells. *Eur. J. Cancer*, **35**, 1274–1280.

Price, S., Burnet, N., Donovan, T., Green, H., Pena, A., Antoun, N., Pickard, J., Carpenter, T., and Gillard, J. (2003). Diffusion tensor imaging of brain tumours at 3t: a potential tool for assessing white matter tract invasion? *Clin. radiol.*, **58**, 455–462.

Swanson, K. R., Alvord, E. C. J., and Murray, J. D. (2002). Virtual brain tumours (gliomas) enhance the reality of medical imaging and highlight inadequacies of current therapy. *Br. J. Cancer*, **86**, 14–18.

Thorogood, P. and Wood, A. (1987). Analysis of in vivo cell movement using transparent tissue systems. *J. Cell Sci. Suppl.*, **8**, 395–413.

Tsuji, T. (1982). Scanning electron microscopy of dermal elastic fibres in transverse section. *Br. J. Dermatol.*, **106**, 545–550.

Wang, H. B., Dembo, M., Hanks, S. K., and Wang, Y. (2001). Focal adhesion kinase is involved in mechanosensing during fibroblast migration. *Proc. Natl. Acad. Sci. U S A*, **98**, 11295–11300.

Wang, W., Wyckoff, J. B., Frohlich, V. C., Oleynikov, Y., Huttelmaier, S., Zavadil, J., Cermak, L., Bottinger, E. P., Singer, R. H., White, J. G., Segall, J. E., and Condeelis, J. S. (2002). Single cell behavior in metastatic primary mammary tumors correlated with gene expression patterns revealed by molecular profiling. *Cancer Res.*, **62**, 6278–6288.

Weiner, R., Schmitt, B., and H., P. (1997). Rowmap–a row-code with krylov techniques for large stiff odes. *Appl. Num. Math.*, **25**, 303–319.

Wilkinson, P. C. and Lackie, J. M. (1983). The influence of contact guidance on chemotaxis of human neutrophil leukocytes. *Exp. Cell Res.*, **145**, 255–264.

Wolf, K., Muller, R., Borgmann, S., Brocker, E. B., and Friedl, P. (2003a). Amoeboid shape change and contact guidance: T-lymphocyte crawling through fibrillar collagen is independent of matrix remodeling by MMPs and other proteases. *Blood*, **102**, 3262–3269.

Wolf, K., Mazo, I., Leung, H., Engelke, K., von Andrian, U. H., Deryugina, E. I., Strongin, A. Y., Brocker, E. B., and Friedl, P. (2003b). Compensation mechanism in tumor cell migration: mesenchymal-amoeboid transition after blocking of pericellular proteolysis. *J. Cell Biol.*, **160**, 267–277.

Wood, A. (1988). Contact guidance on microfabricated substrata: the response of teleost fin mesenchyme cells to repeating topographical patterns. *J. Cell Sci.*, **90**, 667–681.

Wood, A. and Thorogood, P. (1984). An analysis of in vivo cell migration during teleost fin morphogenesis. *J. Cell Sci.*, **66**, 205–222.